

**Transverse spin effects in SIDIS  
at 11 GeV with a transversely polarized target  
using the CLAS12 Detector**

H. Avakian<sup>†</sup>, S. Boyarinov, V.D. Burkert, A. Deur, L. Elouadrhiri, T. Kageya, V. Kubarovsky,  
M. Lowry, B. Musch, A. Prokudin, A. Sandorfi, Yu. Sharabian, S. Stepanyan, M. Ungaro, X.Wei<sup>†</sup>  
Jefferson Lab, Newport News, VA 23606, USA

M. Aghasyan<sup>†</sup>, E. De Sanctis, D. Hasch, L. Hovsepyan, V. Lucherini  
M. Mirazita, and S. Anefalos Pereira, S. Pisano, P. Rossi  
LNF INFN, Frascati, I-00044, Rome Italy

G. Schnell  
The University of the Basque Country, Postal 644, E-48080 Bilbao, Spain  
K. Joo<sup>†</sup>, N. Markov, P. Schweitzer  
University of Connecticut, Storrs, CT 06269, USA

L. Barion, G. Ciullo, M. Contalbrigo<sup>†\*</sup>, P.F. Dalpiaz, P. Lenisa, L.L. Pappalardo, M. Statera  
University of Ferrara and INFN Ferrara, Via Saragat, I-44100, Ferrara, Italy  
G. De cataldo, R. De Leo, L. La Gamba, E. Nappi  
University of Bari and INFN Bari, Via Orabona, I-70125, Bari, Italy  
M. Battaglieri, A. Celentano, R. De Vita, M. Osipenko, G. Ricco, M. Ripani, M. Taiuti  
INFN Genova, Via Dodecaneso, 33 I-16146 Genova, Italy

K. Griffioen  
College of William & Mary, 23187, USA  
V. Bellini, A. Giusa, F. Mammoliti, R. Potenza, G. Russo, L. Sperduto, C. Sutura  
University of Catania and INFN Catania, Via S. Sofia, I-95123 Catania, Italy

R. Perrino  
INFN Lecce, Via Arnesano, I-73100 Lecce, Italy  
K. Hafidi, J. Arrington, L. El Fassi, D. F.Geesaman, R. J. Holt,  
D. H. Potterveld, P. E. Reimer, P. Solvignon  
Argonne National Lab, Argonne, IL 60439, USA

J. Ball, M. Garçon, M. Guidal, S. Niccolai, F. Sabatié  
IPNO (Orsay), SPhN (Saclay) France  
M. Amarian, G. Dodge, G. Gavalian Old Dominion University, Norfolk, VA 23529, USA  
A. D'Angelo, C. Schaerf, I. Zonta  
Dipartimento di Fisica, Università di Roma Tor Vergata,  
INFN Sezione di Roma Tor Vergata, Via della Ricerca Scientifica, I-00133, Rome, Italy

A. Biselli

Fairfield University, Fairfield CT 06824, USA

F. Meddi, G.M. Urciuoli

INFN Roma I, P.le Aldo Moro, I-00185, Roma, Italy

E. Cisbani, A. Del Dotto, F. Garibaldi, S. Frullani

INFN Roma I and Istituto Superiore di Sanita', Viale Regina Elena, I-00161, Roma, Italy

M. Capogni

INFN Roma I and ENEA Casaccia, Via Anguillarese, I-00123, Roma, Italy

E.N. Golovach, G.V. Fedotov, B.S. Ishkhanov, E.L. Isupov, V.I. Mokeev, N.V. Shvedunov

Skobeltsyn Institute of Nuclear Physics and Physics Department at Moscow State University

19899 Vorob'evy gory, Skobeltsyn Nuclear Physics Institute at Moscow State University, Moscow, Russia

A. Puckett Los Alamos National Laboratory, Los Alamos, NM 87545, USA

M. Anselmino, A. Kotzinian, B. Parsamyan,

Università di Torino and INFN, Sezione di Torino, Via P. Giuria 1, I-10125 Torino

A. Bacchetta, A. Courtoy, M. Radici, B. Pasquini

Università di Pavia and INFN Sezione di Pavia, via Bassi 6, 27100 Pavia, Italy

L. Gamberg

Penn State Berks, Reading, PA 19610, USA

## A CLAS collaboration proposal

<sup>†</sup> Co-spokesperson

<sup>\*</sup> Contact: Marco Contalbrigo, INFN Ferrara, Ferrara 44100 Italy.

Email: [contalbrigo@fe.infn.it](mailto:contalbrigo@fe.infn.it)

## Abstract

We propose to study spin azimuthal asymmetries in semi-inclusive DIS (SIDIS) using an 11 GeV polarized electron beam from the upgraded CEBAF facility and the CLAS12 detector equipped with a transversely polarized target. The main focus of the experiment will be the measurement of transverse target single- and double-spin asymmetries (TTSA) in the reaction  $ep^\uparrow \rightarrow ehX$ , where  $h$  is a meson (e.g. a pion or a kaon) and  $X$  is the undetected final state. In particular, three single-spin asymmetries (SSA) will be measured, each providing access to a specific leading-twist parton distribution function (PDF): the transversity, the Sivers function and the so-called “pretzelosity” function. In a transversely polarized nucleon, the Sivers function describes the distribution of unpolarized quarks, whereas the transversity and “pretzelosity” functions describe the distribution of transversely polarized quarks. The joint use of a longitudinally polarized beam and a transversely polarized target will also allow us to measure double-spin asymmetries (DSA) related to an unmeasured leading-twist TMD distribution function describing the distribution of longitudinally polarized quarks in a transversely polarized nucleon (*worm-gear*). The expected asymmetries from the leading-order calculations and Monte Carlo studies are in the range of 2 to 10%, depending on the kinematics and on the models used for the PDFs. The  $x$ ,  $Q^2$ ,  $z$  and  $\mathbf{P}_{h\perp}$  dependences of the TTSAs will be studied in a wide kinematic range.

A total of 110 days of beam time is requested for this experiment.

# Contents

|          |   |           |
|----------|---|-----------|
| <b>1</b> | <b>Introduction</b>   | <b>5</b>  |
| <b>2</b> | <b>Theory and Motivation</b>  | <b>6</b>  |
| 2.1      | The leading-twist TMDs . . . . .  | 6         |
| 2.2      | The SIDIS cross-section . . . . .   | 9         |
| 2.3      | Present Experimental Results on Spin-Azimuthal Asymmetries . . . .                  | 12        |
| 2.4      | The Impact of CLAS12 Measurements . . . . .   | 16        |
| <b>3</b> | <b>Experimental Situation</b>   | <b>20</b> |
| 3.1      | The Present Experiments . . . . .   | 20        |
| 3.2      | JLab Proposals . . . . .  | 20        |
| <b>4</b> | <b>A Dedicated SIDIS Experiment with a Transversely Polarized Target and CLAS12</b> | <b>21</b> |
| 4.1      | The CLAS12 Configuration . . . . .  | 22        |
| 4.1.1    | The HD-Ice Transversely Polarized Target . . . . .                                  | 22        |
| 4.1.2    | Target Polarization Measurements . . . . .  | 28        |
| 4.1.3    | The Impact of Møller Scattering . . . . .   | 29        |
| 4.1.4    | The CLAS12 Particle Identification . . . . .  | 31        |
| 4.1.5    | The CLAS12 RICH detector . . . . .  | 31        |
| 4.2      | The Measurement . . . . .   | 39        |
| 4.2.1    | Event Reconstruction . . . . .  | 39        |
| 4.2.2    | Event Identification . . . . .  | 39        |
| 4.2.3    | Acceptance and Data Analysis . . . . .  | 39        |
| 4.2.4    | Count Rates and Statistical Errors . . . . .  | 44        |
| 4.2.5    | Systematic Errors . . . . .   | 45        |
| 4.3      | Projected Results . . . . .   | 47        |
| 4.4      | Fourier Transformed Cross Sections . . . . .  | 56        |
| <b>5</b> | <b>Summary and Beam Time Request</b>  | <b>59</b> |

# 1 Introduction

One of the main objectives of the Jefferson Lab upgrade is the understanding of the internal structure of the nucleon and nucleus in terms of quarks and gluons, the fundamental degrees of freedom of Quantum Chromodynamics (QCD). The partonic structure of hadrons beyond the collinear approximation, or 3D structure of the nucleon, can be described by two new categories of parton distributions: the transverse momentum dependent parton distributions (TMDs) [1, 2, 3, 4, 5, 6, 7, 8], and the generalized parton distributions (GPDs) [9, 10, 11, 7, 12, 13, 14, 15].

The ultimate knowledge of finding a single parton inside a hadron – involving both momentum and space information – can be encoded in the phase-space distributions of quantum mechanics, such as the Wigner quasi-probability distribution  $W(k_T, b)$ , whose integration over the parton spatial dependence ( $b$ ) leads to the TMDs, while its integration over transverse momentum ( $k_T$ ) provides the parton’s spatial distribution that is relevant to the GPDs. Understanding both the momentum and spatial distribution of a parton inside a hadron in terms of the more general Wigner distributions could be the central object of future studies on partonic structure. The concept of Wigner distributions in QCD for quarks and gluons was first explored in Refs. [16, 7], introducing the definition of a Wigner operator whose matrix elements in the nucleon states were interpreted as distributions of the partons in a six-dimensional space (three position and three momentum coordinates). The link with GPDs was exploited to obtain three-dimensional spatial images of the proton which were interpreted as charge distributions of the quarks for fixed values of the Feynman variable  $x$ .

Significant progress has been recently made in understanding the role of partonic initial and final state interactions [17, 18, 19]. The interaction between the active parton in the hadron and the spectators leads to gauge-invariant transverse momentum dependent (TMD) parton distributions [17, 18, 19, 20, 21, 22]. Furthermore, QCD factorization for semi-inclusive deep inelastic scattering at low transverse momentum in the current-fragmentation region has been established in Refs. [23, 24]. Recently, a complete TMD factorization derivation, in terms of well-defined TMDs with individual evolution properties, was presented by Collins [?]. That formalism has been used to obtain evolved TMDs from fixed-scale fits [?, ?].

This new framework provides a rigorous basis to study the TMD parton distributions from SIDIS data using different spin-dependent and spin-independent observables. TMD distributions (see Table 1) describe different spin-spin and spin-orbit correlations in the momentum space [25, 8, 26, 27]. Similar correlations arise in the hadronization process. One particular case is the Collins  $T$ -odd fragmentation function  $H_1^\perp$  [28], describing fragmentation of transversely polarized quarks into unpolarized hadrons. Knowledge of TMDs is also crucial for understanding phenomena in high energy hadronic scattering processes, such as, the single transverse spin asymmetries [17, 29, 18, 19, 20, 30].

| N/q | U              | L              | T                                 |
|-----|----------------|----------------|-----------------------------------|
| U   | $\mathbf{f_1}$ |                | $h_1^\perp$                       |
| L   |                | $\mathbf{g_1}$ | $h_{1L}^\perp$                    |
| T   | $f_{1T}^\perp$ | $g_{1T}^\perp$ | $\mathbf{h_1} \quad h_{1T}^\perp$ |

Table 1: Leading-twist transverse momentum-dependent distribution functions.  $U$ ,  $L$ , and  $T$  stand for transitions of unpolarized, longitudinally polarized, and transversely polarized nucleons (rows) to corresponding quarks (columns).

We propose a high luminosity ( $5 \cdot 10^{33} \text{ cm}^{-2}\text{s}^{-1}$ ) measurement of transverse target single-spin asymmetries in SIDIS using the CLAS12 detector in Hall B with an 11 GeV longitudinally polarized electron beam and the transversely polarized HD-Ice target. The main goal of this proposal is the study of the  $x$ ,  $Q^2$ ,  $z$ , and  $\mathbf{P}_{h\perp}$  dependences of transverse target single-spin asymmetries (SSAs) and double-spin asymmetries (DSAs). The proposed measurements are essential for the study of the transverse momentum-dependent distributions and, when combined with already approved CLAS12 measurements with unpolarized [31, 32] and longitudinally polarized [33, 34] targets, will constrain all chiral-odd leading twist TMDs in the range of  $Q^2$  from 1 to 8 GeV<sup>2</sup>,  $x$  from 0.05 to 0.6, and  $P_{h\perp}$  up to 1.5 GeV/c. One of the main focuses of the proposed measurement will be the transverse momentum dependence of the underlying TMDs, and in particular of the Sivers function. The same measurement will also provide important information on different sub-leading distribution functions [35, 36].

The CLAS12 detector will provide a unique opportunity to perform the measurements over a wide range of kinematics with a single experiment.

## 2 Theory and Motivation

### 2.1 The leading-twist TMDs

The eight leading-twist TMDs are shown in Table 1. The diagonal elements are occupied by the three fundamental leading-twist parton distribution functions: the *momentum* ( $f_1(x, k_T^2)$ ), the *helicity* ( $g_1(x, k_T^2)$ ) and the *transversity* ( $h_1(x, k_T^2)$ ) distributions. They are the only ones that survive after integration over the intrinsic transverse momentum  $k_T$ , and are all needed for a complete description of the collinear nucleon structure.

The transversity distribution [1, 37] and its first moment, the tensor charge, are as fundamental for understanding of the spin structure of the nucleon as are the helicity distribution  $g_1$  and the axial vector charge. Differently from  $g_1$ ,  $h_1$  is chirally odd, i.e. requires a quark helicity flip that cannot be achieved in inclusive DIS. For

non-relativistic quarks  $h_1$  is equal to the helicity distribution  $g_1$ , thus any differences among the two functions probes the relativistic nature of quarks. The  $h_1$  function has a very different  $Q^2$  evolution than  $g_1$  since there is no gluon transversity in the nucleon. The tensor charge is reliably calculable in lattice QCD with  $\delta\Sigma = \sum_f \int_0^1 dx (h_1^f - \bar{h}_1^f) = 0.562 \pm 0.088$  at  $Q^2=2 \text{ GeV}^2$ , which is twice as large as the value of the axial charge [38]. A similar quantity ( $\delta\Sigma \approx 0.6$ ) was obtained in the effective chiral-quark-soliton model [39].

The off-diagonal TMD distributions for transversely polarized quarks arise from interference between amplitudes with left- and right-handed polarization states, and only exist because of chiral symmetry breaking in the nucleon wave function in QCD. Their study therefore provides a new avenue for probing the chiral nature of the partonic structure of hadrons.

Among the off-diagonal elements, the Sivers function ( $f_{1T}^\perp(x, k_T^2)$ ) is of particular interest. It describes the difference between the probability to find a quark with light-cone momentum fraction  $x$  and transverse momentum  $k_T$  inside a hadron polarized transversely to its momentum direction, and the one where the polarization points in the opposite direction. The Sivers function has been phenomenologically extracted by several groups, mainly from analyzing the azimuthal distribution of a single hadron in SIDIS [40, 41, 42, 43].

Important aspects of the TMD parton distributions, such as gauge invariance, the role of gauge links, and universality, have been explored in recent years [18, 19, 20, 22, 30, 44, 45, 46]. Like the PDFs, the definition of TMDs is closely connected to the factorization of physical cross sections, and it is necessary for the TMDs to include all leading power long-distance contributions to the physical cross sections if they can be factorized. All leading power collinear gluon interactions are summed into the gauge links in the definition of the TMDs. It is the gauge link that makes the TMDs gauge invariant and provides the necessary phase for generating a sizable single transverse spin asymmetry (SSA) in SIDIS and Drell-Yan processes [17, 18, 19, 20, 22, 29]. However, unlike the PDFs, which are universal, the TMDs could be process dependent due to the fact that the initial-state and final-state collinear gluon interactions are summed into two different gauge links. That is, the TMDs extracted from SIDIS could be different from those extracted from Drell-Yan processes because of the difference in gauge links. Although the TMDs are not in general universal, it can be shown from the parity and time-reversal invariance of QCD dynamics that the process dependence of the spin-averaged as well as spin-dependent TMDs involves only a sign change, which was referred to as the parity and time-reversal modified universality [18, 30]. An important example of the modified universality is that the Sivers function extracted from the SIDIS measurements is opposite in sign from the Sivers function extracted from the Drell-Yan process. The test of the sign change of the Sivers function from SIDIS to Drell-Yan is a critical test of the TMD factorization and several Drell-Yan proposals were approved to measure TMDs [47, 48] and perform that test [49]. The possibility of a node in the  $x$ -dependence of the Sivers

function has been discussed in light of this important test [50]. As the Sivers function describes a difference of probabilities it is not necessarily positive definite. Recent measurements of multiplicities and double spin asymmetries as a function of the final transverse momentum of pions in SIDIS at JLab [51, 52] suggest that transverse momentum distributions may depend on the polarization of quarks and possibly also on their flavor. Calculations of transverse momentum dependence of TMDs in different models [53, 54, 55, 56] and on lattice [57, 58] indicate that the dependence of the transverse momentum distributions on the quark polarization and flavor may be very significant. There are some indications that the transverse momentum dependence of the Sivers functions, important for comparison of Sivers function measurements from different processes and the corresponding collinear higher twist, may also not be trivial [59].

Studies of the shape of the proton indicate [60, 61] that for transversely polarized quarks in a transversely polarized nucleon, the shape of the nucleon is reminiscent of a pretzel. The distribution of transversely polarized quarks in a transversely polarized nucleon is described by the TMD  $h_{1T}^\perp(x, k_T^2)$  and its magnitude will thus be related to the “pretzelosity” of the proton [60]. Recently it has been suggested, based on some quark models, that the pretzelosity TMD may also be related to the quark orbital angular momentum (OAM) [62, 63, 64, 65]

$$\mathcal{L}_z^q = - \int dx d^2k_\perp \frac{k_T^2}{2M^2} h_{1T}^{\perp q}(x, k_T^2). \quad (1)$$

The TMD  $h_{1T}^\perp$  corresponds to the amplitude where the nucleon and active quark longitudinal polarizations flip in opposite directions, involving therefore a change by two units of OAM between the initial and final nucleon states. It was shown (see *e.g.* [66]) that in a gauge theory, in general,  $\mathcal{L}_z^q$  may not be related to the total quark contribution to the nucleon spin from a combination of GPDs from Ji’s sum-rule [67].

Another interesting TMD distribution function accessible in studies with transversely polarized nucleons is the *worm-gear*  $g_{1T}^\perp(x, k_T^2)$ . It describes the probability to find longitudinally polarized quarks in a transversely polarized nucleon. Noteworthy, it is the only TMD function not affected by initial- or final-state interactions as it is neither chiral-odd nor T-odd. It can be accessed, in conjunction with the spin-independent fragmentation function  $D_1$ , in double-spin asymmetries with a longitudinally polarized beam and a transversely polarized nucleon.

There have been many interesting model studies recently, see for example [68, 64, 69, 70, 55, 26]. These models and their calculations could play a very important role as a first step to describe the experimental observations, to give an intuitive way to connect the physical observables to the partonic dynamics, and to provide key inputs to the partonic structure of the nucleon. More importantly, very exciting results of TMDs have come from recent lattice QCD calculations [57, 71, 58], indicating that spin-orbit correlations could change the transverse momentum distributions of partons.

## 2.2 The SIDIS cross-section

The SIDIS cross section can be decomposed in terms of Structure Functions [23, 8], each related to a specific azimuthal modulation:

$$\begin{aligned}
\sigma(\phi, \phi_S) \equiv \frac{d^6\sigma}{dxdydzd\phi d\phi_S dP_{h\perp}^2} &= \frac{\alpha^2}{xyQ^2} \frac{y^2}{2(1-\epsilon)} \left( 1 + \frac{\gamma^2}{2x} \right) \\
&\left\{ F_{UU,T} + \epsilon F_{UU,L} + \sqrt{2\epsilon(1+\epsilon)} \cos\phi F_{UU}^{\cos\phi} + \epsilon \cos(2\phi) F_{UU}^{\cos(2\phi)} \right. \\
&\quad \left. + \lambda_e \sqrt{2\epsilon(1-\epsilon)} \sin\phi F_{LU}^{\sin\phi} \right. \\
&\quad + S_L \left[ \sqrt{2\epsilon(1+\epsilon)} \sin\phi F_{UL}^{\sin\phi} + \epsilon \sin(2\phi) F_{UL}^{\sin(2\phi)} \right] \\
&\quad + S_L \lambda_e \left[ \sqrt{1-\epsilon^2} F_{LL} + \sqrt{2\epsilon(1-\epsilon)} \cos\phi F_{LL}^{\cos\phi} \right] \\
&\quad + |S_T| \left[ \sin(\phi - \phi_S) \left( F_{UT,T}^{\sin(\phi-\phi_S)} + \epsilon F_{UT,L}^{\sin(\phi-\phi_S)} \right) \right. \\
&\quad \left. + \epsilon \sin(\phi + \phi_S) F_{UT}^{\sin(\phi+\phi_S)} + \epsilon \sin(3\phi - \phi_S) F_{UT}^{\sin(3\phi-\phi_S)} \right. \\
&\quad \left. + \sqrt{2\epsilon(1+\epsilon)} \sin\phi_S F_{UT}^{\sin\phi_S} + \sqrt{2\epsilon(1+\epsilon)} \sin(2\phi - \phi_S) F_{UT}^{\sin(2\phi-\phi_S)} \right. \\
&\quad \left. + |S_T| \lambda_e \left[ \sqrt{1-\epsilon^2} \cos(\phi - \phi_S) F_{LT}^{\cos(\phi-\phi_S)} + \sqrt{2\epsilon(1-\epsilon)} \cos\phi_S F_{LT}^{\cos\phi_S} \right. \right. \\
&\quad \left. \left. + \sqrt{2\epsilon(1-\epsilon)} \cos(2\phi - \phi_S) F_{LT}^{\cos(2\phi-\phi_S)} \right] \right\}, \quad (2)
\end{aligned}$$

where  $\lambda_e$  refers to the helicity of the electron beam,  $S_L$  and  $S_T$  to the longitudinal and transverse polarization of the target nucleons (with respect to the direction of the virtual photon), and  $\epsilon$  to the ratio of the longitudinal and transverse photon fluxes, which is determined by the kinematics of the lepton. Here,  $q = l - l'$  is the four-momentum of the virtual photon,  $Q^2 = -q^2$ ,  $x = Q^2/2(Pq)$ ,  $y = (Pq)/(Pl)$ ,  $\phi_S$  is the azimuthal angle of the transverse spin in the scattering plane, and  $P$  is the initial nucleon momentum. The azimuthal angle  $\phi$  is defined as the angle between the scattering plane, formed by the initial and final momenta of the electron, and the production plane, formed by the transverse momentum  $P_{h\perp}$  of the observed hadron and the virtual photon (Fig. 1). The azimuthal angle  $\phi_S$  is defined as the angle between the scattering plane and the target spin component transverse to the virtual photon.

The subscripts in the structure functions  $F_{UT,UL,LT}$ , specify the beam (first index) and target (second index) polarization ( $U, L, T$  for unpolarized, longitudinally and transversely polarized targets, and  $U, L$  for unpolarized and longitudinally polarized beam).

At leading twist there are eight contributions related to different combinations of polarization states of the incoming lepton and the target nucleon. They all can be

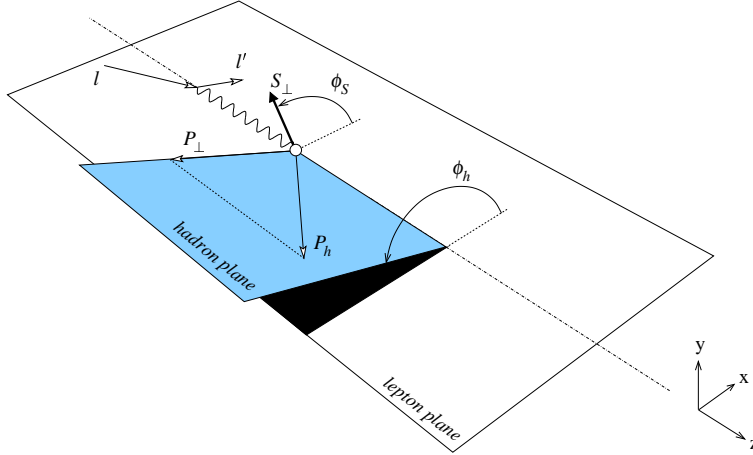


Figure 1: The SIDIS kinematics.

independently measured in SIDIS thanks to their specific azimuthal dependencies. The study of the terms related to unpolarized and longitudinally polarized targets are subject of different CLAS12 proposals [33, 34, 32, 72]. The structure functions factorize into TMD parton distribution and fragmentation functions, and soft and hard parts [23]. For example,  $F_{UT}^{\sin(\phi+\phi_S)}$  can be written as

$$F_{UT}^{\sin(\phi+\phi_S)} = \int \frac{\vec{p}_\perp \cdot \hat{\vec{P}}_T}{M} \times h_1(x, k_T) H_1^\perp(z, p_T) S(\vec{\lambda}_\perp) H_{UT}(Q^2) . \quad (3)$$

The hard factor,  $H_{UT}$ , is calculable in pQCD, and the soft factor  $S(\vec{\lambda}_\perp)$  comes from soft gluon radiation and is defined by a matrix element of Wilson lines in the QCD vacuum [23]. The integral symbol represents integration over the transverse momentum of the initial,  $k_T$ , and scattered  $p_T$  partons and the soft gluon momentum  $\vec{\lambda}_\perp$  [73]. The distribution ( $h_1$ ) and fragmentation ( $H_1^\perp$ ) functions involved depend on the fraction of the proton momentum carried by the struck quark,  $x$ , and of the virtual photon energy fraction carried by the final state hadron,  $z$ , respectively, as well as on the corresponding transverse momenta  $k_T$  and  $p_T$ .

The TMDs define the probability density of finding a (polarized) quark with longitudinal momentum fraction  $x$  and transverse momentum  $k_T$  inside polarized and unpolarized nucleons. For example, the probability of finding an unpolarized quark with longitudinal momentum fraction  $x$  and transverse momentum  $k_T$  inside a transversely polarized target is given by:

$$\Phi^q(x, k_T; S) = f_1^q(x, k_T^2) - \frac{(\hat{P} \times k_T) S_T}{M} f_{1T}^{\perp q}(x, k_T^2) . \quad (4)$$

The Sivers contribution to the  $F_{UT}^{\sin(\phi-\phi_S)}$  structure function, being leading twist, is expected to survive at higher  $Q^2$ . Recently the Sivers asymmetry has been calculated and compared at different scales using the TMD evolution equations applied to previously existing extractions [?].

At large hadron transverse momentum, *i.e.*  $P_{h\perp} \gg \Lambda_{\text{QCD}}$ , the transverse-momentum dependence of the various factors in the factorization formula [23] may be calculated from perturbative QCD. Following arguments in Ji-Qiu-Vogelsang-Yuan [74], the  $\sin(\phi - \phi_S)$  azimuthal asymmetry (*Sivers asymmetry*) has the following behavior at  $\Lambda_{\text{QCD}} \ll P_{h\perp} \ll Q$ ,

$$\langle \sin \phi - \phi_S \rangle|_{P_{h\perp} \gg \Lambda_{\text{QCD}}} \propto \frac{1}{P_{h\perp}} . \quad (5)$$

The above result holds also when the transverse momentum is compatible with the large-scale  $Q$ . Measurement of the  $P_{h\perp}$  dependence of the Sivers asymmetry will, thus, allow to check the predictions of a unified description of SSA by Ji and collaborators [23, 74] and will study the transition from a non-perturbative to a perturbative description. The Sivers asymmetry for semi-inclusive deep inelastic scattering in the kinematic regions of CLAS12 is predicted to be significant ( $\sim 10\%$  at large  $P_{h\perp}$ ) and tends to be larger in the large- $x$  and large- $z$  regions. Measurement of the  $P_{h\perp}$ -dependence of the Sivers asymmetry provides access to the transverse momentum-dependence of the Sivers function. This, in particular, would allow one to determine the first moment of the Sivers function:

$$f_{1T}^{\perp(1)}(x) = \int d^2 k_T \frac{k_T^2}{2M^2} f_{1T}^{\perp(1)}(x, k_T^2) . \quad (6)$$

This moment has a direct connection to so-called soft gluon pole matrix elements [75, 22, 26], and, as a consequence, one may also get a direct connection to the large single spin asymmetries already observed in, for instance,  $p^\uparrow p \rightarrow \pi X$  at Fermilab [76] and at RHIC [77]. Making such a cross check is crucial to understand the various transverse single-spin phenomena in semi-inclusive reactions by means of perturbative QCD. The  $P_{h\perp}$ -dependence will thus provide access to the  $k_T$ -dependence of the Sivers function, which may be relevant to resolve the so-called “sign mismatch”, or the observed mismatch between the signs of the moment of the Sivers function extracted from SIDIS data and twist-3 calculations [59].

Additional leading order azimuthal asymmetries, accessible with transversely polarized target, include the contributions from the worm-gear  $g_{1T}^\perp$ , and pretzelosity  $h_{1T}^\perp$  distribution functions, arising from convolutions with spin-independent,  $D_1^q(z)$ , and spin-dependent,  $H_1^{\perp q}(z)$ , (Collins) fragmentation functions, respectively [28, 4, 3, 17, 19, 78, 79].

A full program to extract TMDs from measurements requires coverage of a large kinematic range in  $x$ ,  $z$ , and  $P_{h\perp}$  along with sensitivity on  $Q^2$  dependence, very good

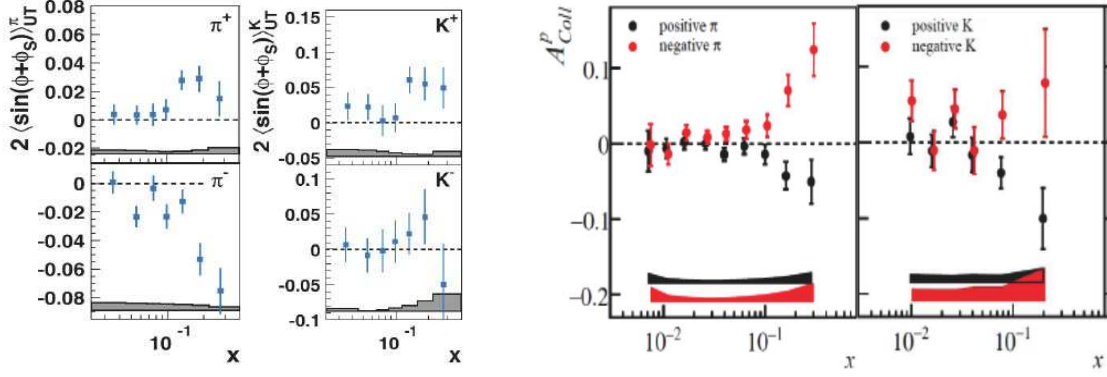


Figure 2: Collins asymmetries measured for identified charged hadrons at HERMES [83] (Left) and COMPASS [86] (Right).

hadron identification (to allow *flavor tagging*), and the use of polarized beam and polarized targets (both longitudinal and transverse polarizations).

## 2.3 Present Experimental Results on Spin-Azimuthal Asymmetries

During the last few years, the first results on transverse SSAs have become available [80, 81, 82, 83, 84, 85]. HERMES and COMPASS measurements for the first time directly indicated significant azimuthal moments generated both by the Collins and the Sivers effects.

The Collins asymmetry  $A_{UT}^{\sin(\phi+\phi_S)}$  has been measured to be non-zero and opposite in sign for opposite charge pions, see Fig. 2. A significant asymmetry was measured recently by Belle [89, 90, 91], indicating that the Collins function  $H_1^\perp$  is indeed large. The SIDIS result is an indication that favored and un-favored Collins fragmentation functions are opposite but of similar magnitude, an observation compatible with the measurements done at  $e^+e^-$  machines [89, 90, 91].

The extraction of the transversity from  $A_{UT}^{\sin(\phi+\phi_S)}$  requires parameterizations for the unpolarized distribution and fragmentation functions along with approximations for the essentially unknown polarized T-odd chiral-odd Collins fragmentation function  $H_1^\perp$ . The Collins function for pions was calculated in a chiral invariant approach at a low scale [92]. It was shown that at large  $z$  the function rises much faster than previously predicted [93, 94] in the analysis using the HERMES data on target SSA. The first extraction of the transversity distribution, together with the Collins fragmentation function, has been carried out recently [95, 87] through a global fit of the BELLE data from  $e^+e^-$  annihilation and the HERMES [80] and COMPASS [81, 82, 96] data on semi-inclusive DIS, see Figs. 3-4.

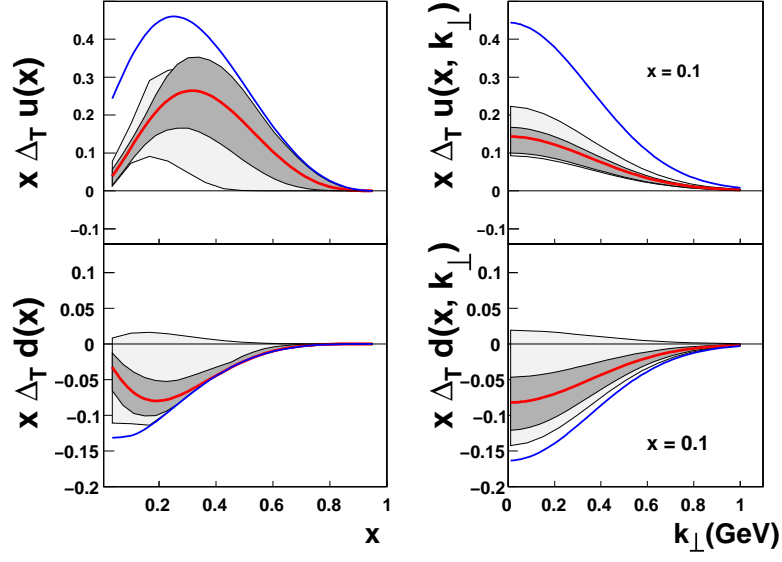


Figure 3: Transversity distribution functions for  $u$  and  $d$  flavors as extracted in [87].

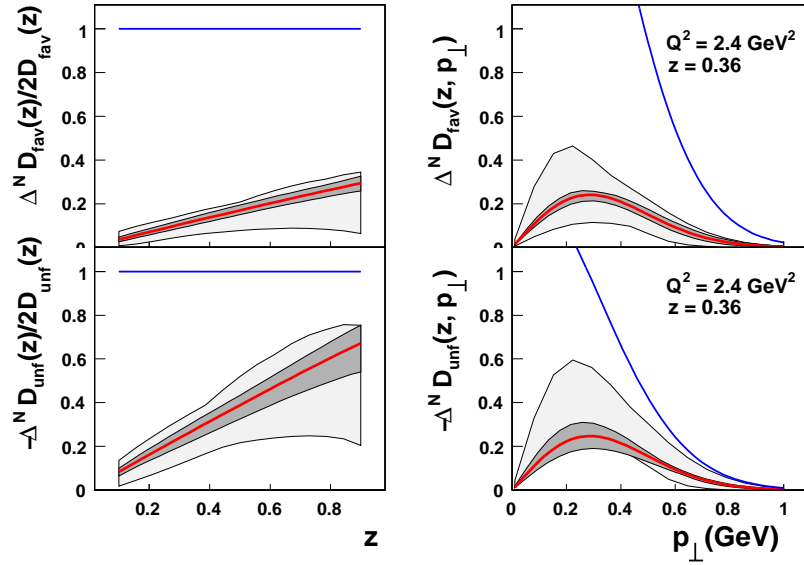


Figure 4: Favored and unfavored Collins fragmentation functions as extracted in [87].

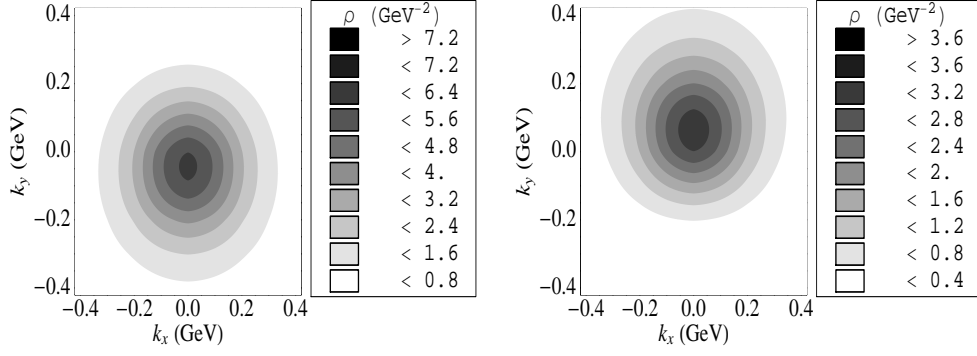


Figure 5: Spin density in the transverse-momentum plane for unpolarized quarks in a transversely polarized nucleon [70]. The left panel is for up quarks, and the right panel for down quarks.

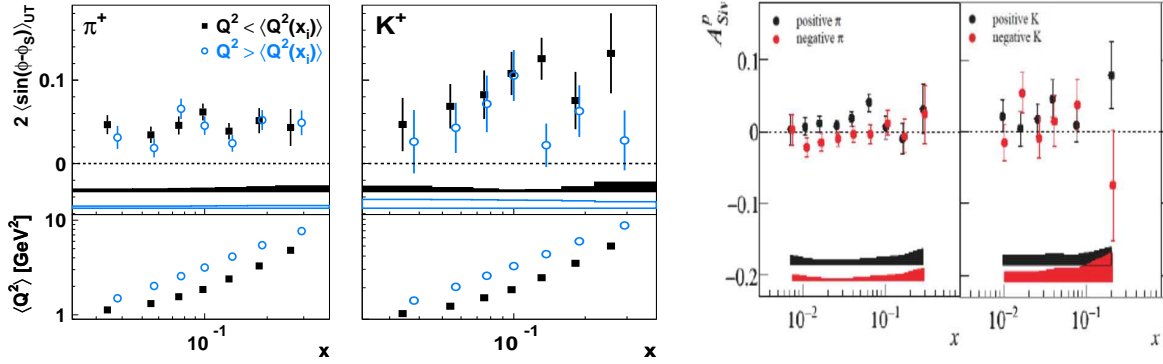


Figure 6: (Left) Sivers asymmetries measured for positive pions and kaons in two  $Q^2$  ranges at HERMES [88]. The bottom panels show the average  $Q^2$  values of the two ranges, which differ by a factor close to 2 in each  $x$ -bins. (Right) Sivers asymmetries measured for identified charged hadrons at COMPASS [86].

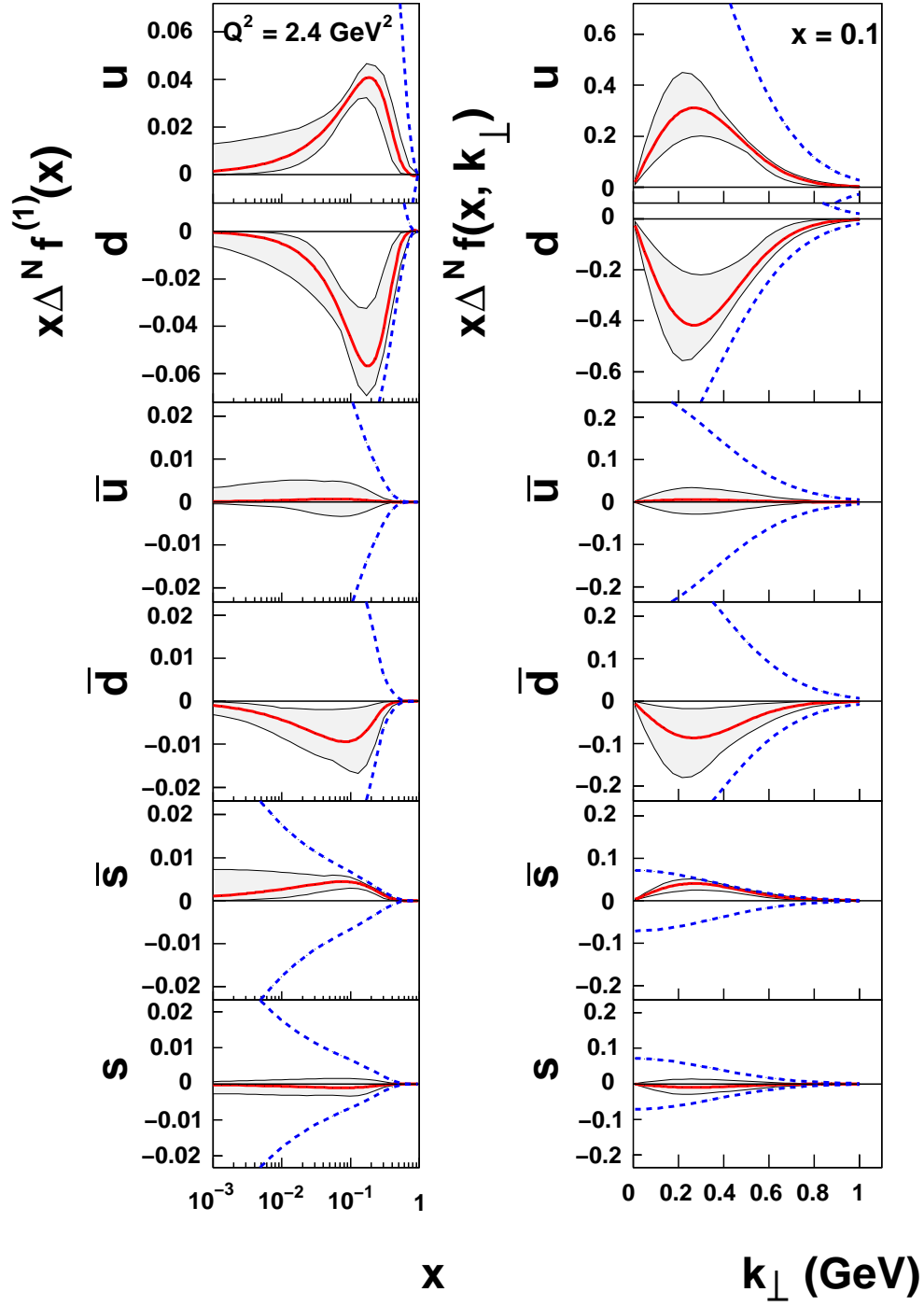


Figure 7: Sivers function for  $u$ ,  $d$ , and  $s$  flavors as extracted in [43].

The SSA for positive kaons is similar to that of positive pions in sign and magnitude, a result compatible with the dominance of the  $u$ -flavor in lepto-scattering over a proton target, see Fig. 2. However, at HERMES the signal for  $\pi^-$  and  $K^-$  are found to follow a different behavior, the former being large and negative, the latter being basically compatible with zero with a hint to be positive [83]. The result would be interesting since the  $K^-$  has no valence quarks in common with the target proton and sea quark transversity is expected to be small, thus  $K^-$  brings specific sensitivity on rank-2 Collins function. Note that the knowledge of the Collins function has an impact on the extraction of all the chirally-odd TMD parton distributions. The results for  $K^-$  are still controversial, since COMPASS data [86] can not prove or disprove it, although seem to not support the HERMES hint, see Fig. 2. The issue can be solved only by novel high-precision experiments.

In SIDIS, substantial Sivers amplitudes  $A_{UT}^{\sin(\phi-\phi_S)}$  were observed in positive hadron production. However, the measurements of HERMES [88] and COMPASS [84] experiments on a proton target are only marginally compatible: the asymmetries measured by COMPASS are somewhat smaller, and seem to indicate an unexpected dependence on  $W$ , the mass of the hadronic final state. Measurements of Sivers amplitudes at HERMES on proton target and COMPASS on (isoscalar) deuteron target are consistent with model calculations (Fig. 5) and lattice calculations indicating opposite signs for the Sivers functions for  $u$  and  $d$  quarks. The Sivers effect, proposed as a possible explanation of the SSA in hadron-hadron collisions, generates SSA in SIDIS reactions for positive kaons which are found larger than for positive pions, see Fig. 6. The difference concentrate at low- $Q^2$ , a possible indication of the presence of higher-twist effects in the kaon sector [88]. The results for negative kaons are not conclusive due to the limited statistics [86].

A recent extraction of the Sivers function for  $u$ ,  $d$ , and  $s$  flavors, also based on the SIDIS results from HERMES and COMPASS, is shown in Fig. 7. The data available, however, is not enough to make statistically significant predictions in the valence region, where the effects are large.

## 2.4 The Impact of CLAS12 Measurements

The effects related to orbital motion of quarks, and in particular the correlations of spin and transverse momentum of the quarks, play an important role especially in the valence region. It was shown that spin-orbit correlations may lead to a significant contribution to partonic momentum and helicity distributions [97] in the large- $x$  limit.

The goal of our proposed experiment is to gather a precise SIDIS data set in the region  $0.1 \leq x \leq 0.6$ ,  $0 \leq P_{h\perp} \leq 1.5$  GeV/c, and  $0.3 \leq z \leq 0.7$ .

Significantly high-statistics CLAS12 data, especially in the intermediate-to-large  $x$  region, will enable the extraction of the  $x$ ,  $z$  and  $P_{h\perp}$  dependences for different azimuthal moments in a wide kinematic range, allowing the source of the observed SSA to be revealed, and the underlying distribution functions to be extracted. In par-

| TMD            | $\langle k_T \rangle$<br>in GeV | $\langle k_T^2 \rangle$<br>in GeV <sup>2</sup> | $\frac{4\langle k_T \rangle^2}{\pi\langle k_T^2 \rangle}$ | $\frac{\langle k_T^2 \rangle}{\langle k_{Tf_1}^2 \rangle}$ |
|----------------|---------------------------------|--|---|--|
| $f_1$          | 0.239                           | 0.080  | 0.909   | 1.00   |
| $g_1$          | 0.206                           | 0.059  | 0.916   | 0.74   |
| $h_1$          | 0.210                           | 0.063  | 0.891   | 0.79   |
| $g_{1T}^\perp$ | 0.373                           | 0.176  | 1.007   | 2.20   |
| $h_{1L}^\perp$ | 0.373                           | 0.176  | 1.007   | 2.20   |
| $h_{1T}^\perp$ | 0.190                           | 0.050  | 0.919   | 0.63   |

Table 2: Predictions for the transverse momentum dependence of the T-even TMDs from the constituent quark model [55]. (Left) The mean transverse momenta and the mean square transverse momenta: if the transverse momenta in the TMDs were Gaussian, then the result for the ratio in the last row would be unity. (Right) Mean square transverse momenta of T-even TMDs in units of the mean square transverse momenta of  $f_1$ , denoted as  $\langle k_{Tf_1}^2 \rangle$ . These ratios are considered to be a more robust model prediction.

ticular, the combined analysis of the future CLAS12 data on  $A_{UT}$  and of the previous HERMES and COMPASS measurements in the small- $x$  domain, will provide information on the Sivers function, shedding light on the correlations between transverse spin and transverse momenta of quarks, and on the transversity function, significantly constraining its first moment related to the nucleon tensor charge.

SIDIS measurements with a joint use of a transversely polarized target and a longitudinally polarized beam provide access to the leading-twist TMD  $g_{1T}^q(x)$ . Significant  $A_{LT}$  double-spin asymmetries were predicted recently for the CLAS12 kinematics (see Fig. 8).

The width of the  $k_T$  distribution for different partonic distributions can be different. For example, values for different T-even TMDs, computed [69] in the constituent quark model [55], are listed in Table 2. Values normalized to the width of the unpolarized distribution function are listed in the same Table.

A common assumption is the Gaussian ansatz for the transverse momentum dependence of distribution and fragmentation functions with the average  $P_{h\perp}$  of hadrons produced in SIDIS given by

$$\langle P_{h\perp}(z) \rangle = \frac{\sqrt{\pi}}{2} \sqrt{z^2 \langle k_T^2 \rangle + \langle p_T^2 \rangle}. \quad (7)$$

In the approximation of flavor and  $x$  or  $z$ -independent widths, a satisfactory description of HERMES deuteron data on average  $P_{h\perp}$  [98] was obtained [99] with

$$\langle k_T^2 \rangle = 0.33 \text{ GeV}^2, \quad \langle p_T^2 \rangle = 0.16 \text{ GeV}^2. \quad (8)$$

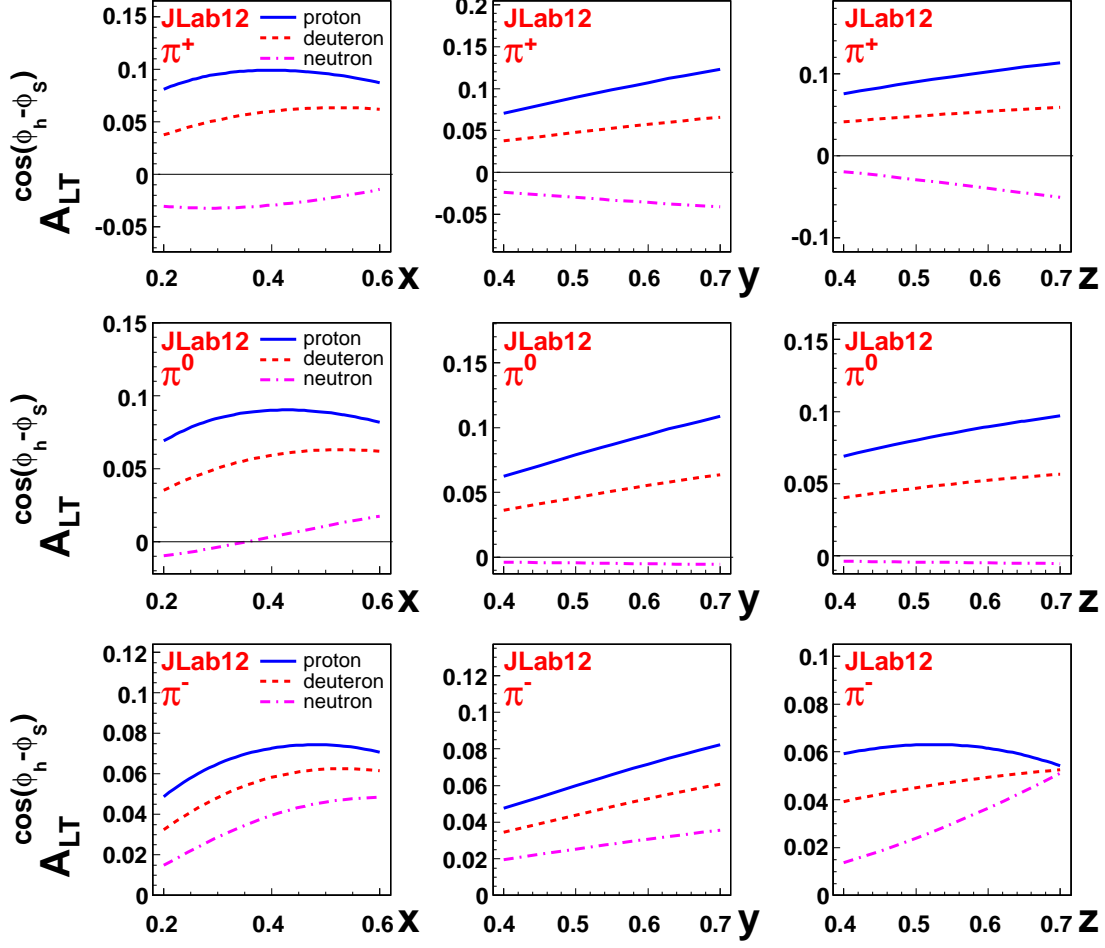


Figure 8: Predicted dependence of  $A_{LT}^{\cos(\phi_h - \phi_s)}$  on  $x$ ,  $y$  and  $z$  with  $|\mathbf{P}_{T,min}| = 0.5$  GeV/c for CLAS12 kinematics.

Very similar results were obtained in Ref. [40] from a study of EMC data [100] on the Cahn effect. Although the ansatz seems to describe satisfactorily the present available data sets [68], it has to be considered as an approximation.

A comprehensive study of the nucleon structure should consider the role of the quark flavor. The use of different targets in conjunction with the detection of various hadrons in the final state provide access to statistical information about the flavor of the struck quark. In particular, kaons provide enhanced sensitivity on strangeness in the matter (partonic sea of the nucleon) and in the vacuum (through fragmentation). Kaon detection is generally challenged by the about one order of magnitude larger flux of pions. Thus very little is known about the spin-orbit correlations related to the strange quark. Only recently dedicated measurements have become available and, despite the limited statistical accuracy, in most of the cases they show surprising results. This is an indication of a non trivial role of the sea quarks in the nucleon, or of a peculiar behavior of the fragmentation mechanism in the presence of strange quark. Moreover a hint exists that kaons provide enhanced sensitivity on higher-twist effects [88]. The interpretation would become possible only in the presence of high-luminosity large-acceptance experiments able to explore the relevant kinematic dependences in conjunction with an efficient hadron identification. Examples of wanted information are a precise  $Q$ -dependence to isolate higher-twist effect and an extended  $P_{h\perp}$ -dependence to map the transient between perturbative and non-perturbative regime.

Very little is known about polarization dependent fragmentation functions (i.e. Collins), but an effort is being pursued to extract them from the large sample of data collected at B-factories [101, 102]. Very precise information on the fragmentation process is anticipated in the next future thanks to the approval of Super B-factories. The detailed study can be completed only by SIDIS measurements, which constrain the fragmentation functions at much lower center-of-mass energy with specific flavor sensitivity (not accessible in  $e^+e^-$  reactions). The detailed knowledge of the fragmentation process would reflect on the precise determination of parton distributions only at experiments with enough statistical precision and flavor sensitivity, like CLAS12 with a RICH detector dedicated to hadron identification.

The CLAS12 TTSA AUT measurements, in conjunction with the study of hadron multiplicities and unpolarized azimuthal modulations in a large range of kinematic variables ( $x, Q^2, z, P_{h\perp}$ ), will provide important input for the study of the transverse momentum dependence of underlying TMDs.

One of the main sources of uncertainties for pions is the fraction of pions coming from vector meson decays. Since the Collins asymmetry has a significant dependence on the type of a produced hadron, pions produced from rho decays will have very different moments compared to direct pions. The large acceptance of CLAS12 detector allows the simultaneous study of vector meson decays, substantially reducing the related source of systematics. Moreover, measurements with kaons, which have a much smaller contribution from vector meson production, can help in understand-

ing the underlying dynamics of the part of measured asymmetries due to Collins fragmentation mechanism.

In summary, the measurements of single and double spin asymmetries for pions and kaons in a large range of kinematic variables ( $x$ ,  $Q^2$ ,  $z$ ,  $P_{h\perp}$ ) combined with measurements with unpolarized targets, will provide detailed information on the flavor and polarization dependence of the transverse momentum distributions of quarks in the valence region and, in particular, on the  $x$  and  $k_T$  dependence of the leading TMD parton distribution functions of  $u$  and  $d$  quarks. Such measurements would allow for detailed tests of QCD dynamics in the valence region, complementing the information obtained from inclusive DIS. They would also serve as novel tools for exploring nuclear structure in terms of the quark and gluon degrees of freedom.

The combination of all 3 target polarization states (U, L, T) opens access to study of single- and double-spin asymmetries, involving essentially unexplored chiral-odd and time-reversal odd distribution functions, providing detailed information on the quark transverse momentum and spin correlations [28, 3, 4, 29, 103]. The list includes transversity [1, 37], Sivers [104, 17, 18, 19], “pretzelosity” [4], worm-gear  $g_{1T}^q(x)$  [105], and Collins [28] functions.

## 3 Experimental Situation

### 3.1 The Present Experiments

Target spin asymmetries have been published by the HERMES Collaboration on the proton [80, 88, 83] and the COMPASS collaboration on deuterium and proton targets [81, 84]. Kinematics at HERMES and in particular at COMPASS is limited to relatively low  $x$ , where the spin-orbit correlations are not expected to be large. In 2010 COMPASS got one additional year of data-taking with transversely polarized proton target. The foreseen gain in statistics is a factor three with respect the publication [84]. At JLab, an experiment has been done in Hall-A with transversely polarized  $^3\text{He}$  target [106] and an experiment is foreseen to run in the fall of 2011 with transversely polarized HD-Ice target [107, 108].

### 3.2 JLab Proposals

At Jefferson Lab there are two closely-related proposals approved to measure SSA with a transversely polarized  $^3\text{He}$  target in Hall-A [109, 110, 111] and a new proposal is being prepared for measurements with a transversely polarized  $\text{NH}_3$  target [112]. The future data from Hall-A experiments will be complementary to those from the proposed CLAS12 measurement with transversely polarized hydrogen target.

The large acceptance of CLAS12 will allow measurements of SIDIS pions over a wide range in  $x$ ,  $Q^2$  and hadron transverse momenta, where the spin-orbit correlations and corresponding TTSA are expected to be significant. The crucial advantages of

the proposed configuration using HD-Ice target is the large acceptance (no strong holding field is required) and the negligible nuclear background, in particular for large  $P_{h\perp}$ . Wide acceptance of the HD-Ice increases the kinematical coverage of measurements, in particular at large  $Q^2$ , providing a wider range in  $Q^2$  allowing studies of evolution effects and control possible higher twist contributions. It has been demonstrated that by using QCD evolved TMDs one can explain observed discrepancies between HERMES and COMPASS data. Predictions have been made for non-trivial behavior of Sivers asymmetry as a function of  $Q^2$  [?].

With respect to nuclear targets ( $\text{NH}_3$ ,  $\text{ND}_3$ ), HD-Ice dilution factor is a factor of 2 better at small  $P_{h\perp}$  of hadrons, and goes up to a factor of 6 at  $P_{h\perp} > 0.8$  GeV [113]. Good dilution factor at large  $P_{h\perp}$  is crucial for studies of transverse momentum dependence of TMDs, which is one of the main goals of our proposal. The CLAS12 spectrometer equipped with a RICH detector, would allow a clean separation between pions, kaons and protons in a wide momentum range (1-10 GeV/c), thus providing flavor-tagging capabilities. In addition, wide acceptance and the capability to measure multi-particle final states will allow the simultaneous measurements of different exclusive vector mesons, important for understanding the background contributions to the Collins and Sivers asymmetries. Projected statistical errors for this proposal are shown in Section 4.3.

## 4 A Dedicated SIDIS Experiment with a Transversely Polarized Target and CLAS12

The main goal of the proposed experiment is to measure the  $x$ ,  $Q^2$  and  $P_{h\perp}$  dependences of the target single- and double-spin asymmetries in the accessible kinematics (Fig. 9). The target single spin asymmetry (TSSA or  $A_{UT}$ ) will be calculated as:

$$A_{UT} = \frac{1}{fP_t} \frac{(N^+ - N^-)}{(N^+ + N^-)}, \quad (9)$$

where  $P_t$  is the target polarization (with respect to the electron beam direction),  $f$  is the dilution factor, i.e. the fraction of events from the polarized material of interest (H or D), and  $N^{+(-)}$  are the charge-normalized extracted number of  $ep^\uparrow \rightarrow ehX$  events for opposite orientations of the transverse spin of the target.

The joint use of a transversely polarized target and a longitudinally polarized beam will also allow us to measure the double-spin asymmetry (TDSA or  $A_{LT}$ ) in the same kinematic region. These quantities are directly sensitive to the model descriptions of the corresponding TMDs and will be measured as:

$$A_{LT} = \frac{1}{fP_B P_t} \frac{(N^{+\uparrow} + N^{-\downarrow}) - (N^{+\downarrow} + N^{-\uparrow})}{(N^{+\uparrow} + N^{-\downarrow}) + (N^{+\downarrow} + N^{-\uparrow})}, \quad (10)$$

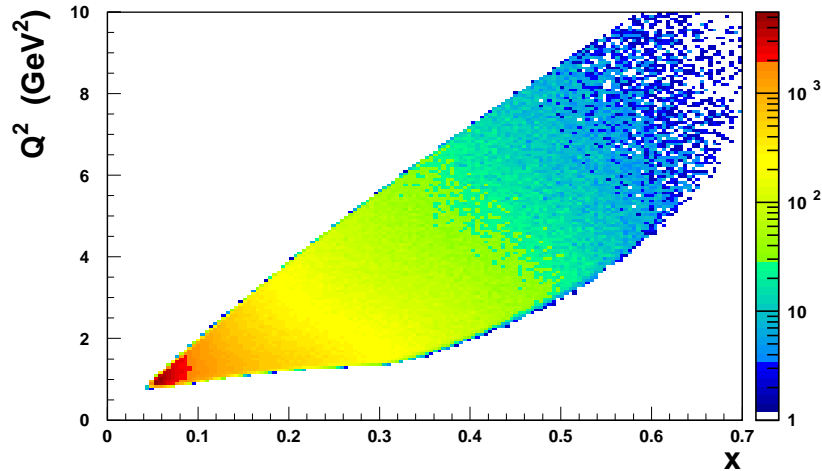


Figure 9: Kinematic coverage of CLAS12 with the transverse target.

where  $P_B$  is the electron beam polarization, and  $N^{\pm\uparrow\downarrow}$  is the extracted number of  $ehX$  events for positive (+) or negative (−) helicities of the beam electrons and transverse ( $\uparrow, \downarrow$ ) target polarizations.

The proposed experiment will provide statistically significant measurements of the kinematic dependences of the target TSSA and the TDSA in pion and kaon lepto-production in SIDIS in the valence region.

## 4.1 The CLAS12 Configuration

The proposed experiment will use the upgraded CLAS12 spectrometer completed by a RICH detector for hadron identification, together with the transversely polarized HD-Ice target, which will include a compensation magnet to shield the target region from the central solenoid so the transverse target magnet can operate.

### 4.1.1 The HD-Ice Transversely Polarized Target

A transversely polarized target in a frozen-spin state, such as the HD-Ice target, requires only relatively small holding fields, which greatly mitigates background problems associated with beam deflection due to the large magnetic fields. This potentially allows to avoid installation of the magnetic chicane to bend the electron beam, deflected by the strong holding field of traditional targets, also generating additional

bremssstrahlung. In addition, the HD-Ice target has limited dilution. The only non polarizable nucleons are associated with the target cell and these can be sampled and subtracted in conventional empty-cell measurements. At the same time, the low  $Z$  results in a long radiation length and comparatively few bremssstrahlung photons.

The factors affecting target polarization are complex and intertwined. At BNL, HD target polarizations of 60% H and 35% D were achieved in photon experiments with spin relaxation times in excess of a year. Hydrogen relaxation times require fields  $\int BdL = 0.050$  T-m, which is about 30 times less than a dynamically polarized ammonia target.

The HD-Ice target has been developed for tagged photon beam operation and is now in use with the CLAS detector employing a new In-Beam-Cryostat(IBC) and the tagged photon facility in Hall B. The target has been used successfully to measure beam-target double polarization asymmetries on protons and on neutrons (deuterium). A tagged photon rate of  $10^8$  per second has been used over many weeks of operation without measurable polarization decays due to beam heating or radiation damage. While the operation in photon beam showed very promising performance of the HD-Ice target, the use of the HD target material in electron beams requires modifications to the heat extraction from the HD material, which was designed for the low beam power when operating the target in photon beams. This requirement affects two technical design aspects of the target for use with intense electron beams, (1) the cooling power of the CLAS IBC and (2) the heat extraction and transport from the HD material to a heat sink. It may also affect (3) the decay time constants of the HD material due to possible more severe radiation damage. An electron beam test was conducted in March in Hall B to obtain empirical information about modifications to the IBC to deal with (1) and (3). The results are briefly summarized here:

- In preparation for the electron beam test, the cooling power of the IBC was increased 3-fold using additional roots pumps. This allowed to keep the cryostat temperature below 160mK using electron currents of 1nA rastered over the 1.5cm diameter target front face. This will be adequate to operate the IBC at luminosities of up to  $L=4 \cdot 10^{33} \text{ cm}^{-2}\text{s}^{-1}$ . However, an additional factor of 3 improvement in cooling power is achievable with the existing IBC and pumping units.
- Heat extraction from the HD material is currently achieved with hundreds of thin aluminum wires of high purity. This design was optimized for photon running and is known to be insufficient for heat extraction with the much higher energy deposition during electron operation. A different design and some R&D work will be needed to develop a new target cell with much improved heat extraction. This could not be done in time when the electron test was conducted. The beam test was therefore limited to low current operation (0.25-1.0 nA). Even at operation of 1nA or less local heating of the HD cell was present that

caused polarization decays during beam operation.

- The most important result from the test is due to possible radiation damage. This was tested by exposing the target to 1nA beam current over a 12 hours period. After this beam exposure, the beam was turned off and the relevant time constant T1 was determined. Due to the very long time constant and uncertainties in the NMR measurement only a lower limit of  $T1 > 50$  days could be established.

To avoid radiation damage to the target the beam will be rastered over the target surface in a spiral pattern. The beam position is measured indirectly by recording the simultaneous currents of the raster magnet. These values can be used off-line to correct for effects of the raster on the vertex z-position. The raster magnets may be also used to give a small angle ( $\sim 0.1^\circ$ ) to the incident electron beam, so that beam at target center will be collinear with the z-axis to confine bremsstrahlung photons into the beam pipe.

The main result of the electron beam test strongly indicates that radiation damage is not causing a rapid decay of the hydrogen polarization at luminosities that are anticipated for this proposal. A remaining technical problem is the heat extraction from the HD material that may require specific R&D work and a refined beam rastering system for use in intense electron beams. As a consequence the present proposal assumes a target wider but not longer than the present one.

The composition for a 5 cm solid HD target with 2.5 cm diameter is shown in the Table 3. Frozen-spin HD, thus, provides a very attractive alternative for electron experiments in particular with transversely polarized targets.

Table 3: HD-Ice target materials

| Material                        | gm/cm <sup>2</sup> | mass fraction (%) |
|---------------------------------|--------------------|-------------------|
| HD                              | 0.735              | 78%               |
| Al                              | 0.139              | 15%               |
| C <sub>2</sub> ClF <sub>3</sub> | 0.065              | 7%                |

The baseline of CLAS12 detector is based on two superconducting magnets. The large 2 T toroid magnet is used by the forward spectrometer as particle momentum analyzer. The 5 T main solenoid of the central detector allows particle momentum determination in the backward region and constrains the large Møller background within the beam pipe.

The insertion of a transverse target in CLAS12 requires a volume where the longitudinal field of the main solenoid is shielded. In the shielded region a transverse target magnet can operate. A solution for a 3 T field and 10 cm long target was proposed at PAC38 to work at  $10^{34} \text{ cm}^{-2}\text{s}^{-1}$  luminosity.

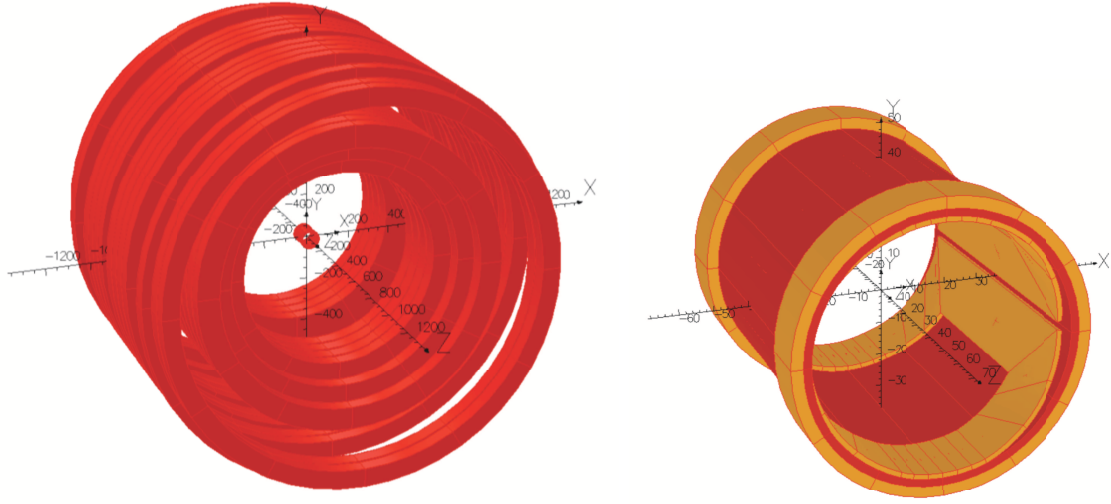


Figure 10: (Left) The HD-Ice superconducting magnetic system surrounds the target at the center of the CLAS12 central detector solenoid. (right) The HD-Ice magnetic system comprises, moving outward from the beam line, the HD-Ice holding field saddle coil (brown), the compensating solenoid (red), and the Helmholtz coil (brown). Only the coils of the magnets are shown.

The recent HD-Ice test with electron beam indicates that the relaxation time of the polarization is not significantly altered by the beam exposure but the heat extraction from the HD material has to be improved. To account for this, a target not-longer than the present one (5 cm) and thus a luminosity of  $5 \cdot 10^{33} \text{ cm}^{-2}\text{s}^{-1}$ , more than an order of magnitude lower than the one affordable with the CLAS12 detector, is here assumed.

In this condition the requirements for the magnetic configuration to shield the longitudinal field of the main solenoid in the target region are less stringent. The Møller background reduces proportionally to the luminosity and can be contained with a limited solenoidal field: ongoing MC studies show that a 2 T field would be enough, see Sec. 4.1.3. The shorter target allows a better compromise between acceptance and holding field uniformity.

In the present design the longitudinal field compensation and the transverse field are generated by superconducting coils internal to the HD-Ice liquid helium can, with almost no impact on the CLAS12 detector configuration. The proposed HD-ice magnet design is basically an enhanced version of the present coil system already in use with the current HD-Ice.

The HD-Ice target requires a highly (better than  $10^{-3}$ ) uniform field for polarization measurement by NMR technique. This is accomplished by the central detector solenoid, able to provide a field uniformity better than  $10^{-4}$  in the limited target vol-

ume. As a consequence, the present long NMR solenoid coil inside the liquid helium can of the HD-Ice cryostat can be shortened to become part of the longitudinal field compensating system, designed to provide a open forward acceptance greater then 35 degrees. The system is completed by an Helmholtz pair of coils, which improves field uniformity and concentrates the material budget in the not-crucial 35-50 degrees transient between current region (forward detector for SIDIS kinematics) and recoil region (central detector for DVCS recoiling proton). The adopted superconducting magnetic configuration, optimizing the acceptance, field uniformity and the material budgetis shown on Fig. 10.

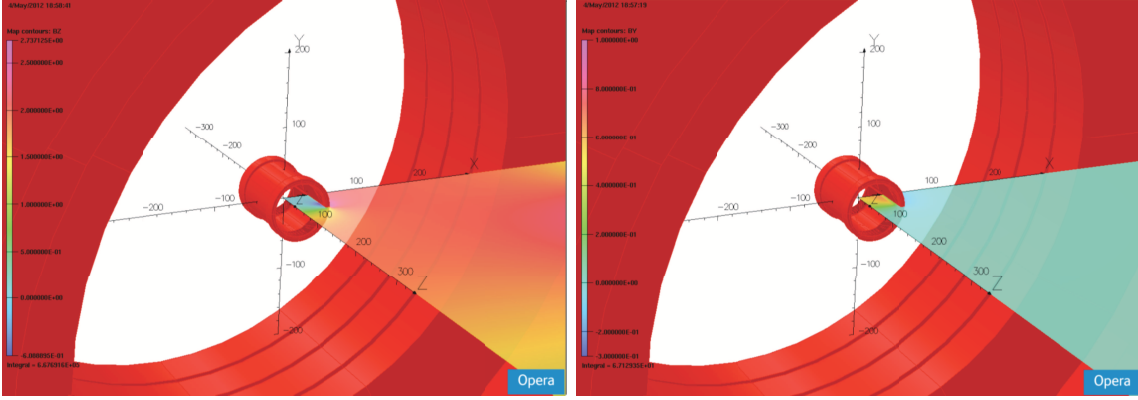


Figure 11: (Left) the 2 T longitudinal field component is almost compensated to zero internal to the HD-Ice magnetic system. (Right) The 0.5 T transverse target holding field is limited to a small volume around the HD-Ice target.

The compensating system is designed to not interfere with the CLAS12 forward acceptance up to angles greater than 35 degrees. It allows the detection of DVCS recoil protons, although with a limited resolution due to the additional material budget associated with the superconducting coil intercepting the recoil proton acceptance. A saddle coil has been added to the system to provide up to 0.5 T transverse field holding the target polarization. The main parameters of the correction magnets are listed in Table 4. The resulting main field components are depicted in Fig. 11.

An interesting parameter is the uniformity of the transverse field holding the target polarization. The surviving longitudinal component of the field in the target volume is not higher than 5 mT for a target length up to 5 cm. Experimentally the target transverse polarization is defined with respect to the beam, whereas the component relevant to theory is the one transverse to the virtual photon. The angle between the beam and the virtual photon is approximately given by  $\sin \theta_{e\gamma^*} \approx \gamma \sqrt{1-y}$  with  $\gamma = 2xM/Q$  and M the proton mass. As a consequence, the target spin actually has a longitudinal component (with respect the virtual photon), which can be as high as  $\pm 15\%$ . The influence on transverse analyses has been studied in detail at HERMES [83, 88], and quantified as negligible. This fixes the order of magnitude

Table 4: Main parameters of the magnet assembling.

| parameter                            | Central detector<br>solenoid (ideal) | Saddle<br>coil | Compensat.<br>solenoid | Compensat.<br>Helmholtz |
|--------------------------------------|--------------------------------------|----------------|------------------------|-------------------------|
| inner radius (mm)                    | 471                                  | 35.8           | 37.4                   | 38.4                    |
| outer radius (mm)                    | 650                                  | 37.4           | 38.4                   | 41.8                    |
| length (mm)                          | 1225                                 | 100            | 100                    | 15                      |
| current density (A/mm <sup>2</sup> ) | 18.2                                 | 730            | 730                    | 730                     |

of the tolerable longitudinal field component into the target volume, which is much higher than the one obtained with the present configuration and a transverse field of 0.5 T.

The static forces acting on the coils of the HD-Ice magnetic system were evaluated to be smaller than 10 MPa, a value well below the 300 MPa tensile strength of the G10 epoxy usually used in superconducting coils assembling. Small misalignments, of the order of 1 mm, of the HD-Ice target system with respect the magnetic center of the central detector solenoid do not generate significant forces as the target sits in a region of pretty uniform field.

The load line of the compensating solenoid are shown in Fig. 12, where different superconducting NbTi wire performances are reported: the SUPERCON 0.229 wire used in the CLAS12 target, the SUPERCON wire used by the PAX experiment at FZJ (VSF/SSCI), together with the F54 wire by BRUKER/EAS and the OK54 wire by LUVATA/OUTOKUMPU. The working point at 730 A/mm<sup>2</sup>, corresponding to the proposed configuration, is below the critical current of commercially available superconducting wires, in particular the one used for the present HD-Ice run at CLAS. As a quench can not be excluded due to external accident, the coils were dimensionated in order to allow the use of a standard quench protection. From the magnetic point of view, the safety margin gives freedom in future geometry optimization for i.e. a reduction of the material budget or a better compromise between field uniformity and acceptance.

In conclusion, a magnetic system internal to the liquid helium can of the HD-Ice target can be used to compensate the central detector longitudinal field in the target volume. The coils can be wound with existing standard commercial wires and work with an acceptable safety margin. Work is in progress to optimize the performances of the system.

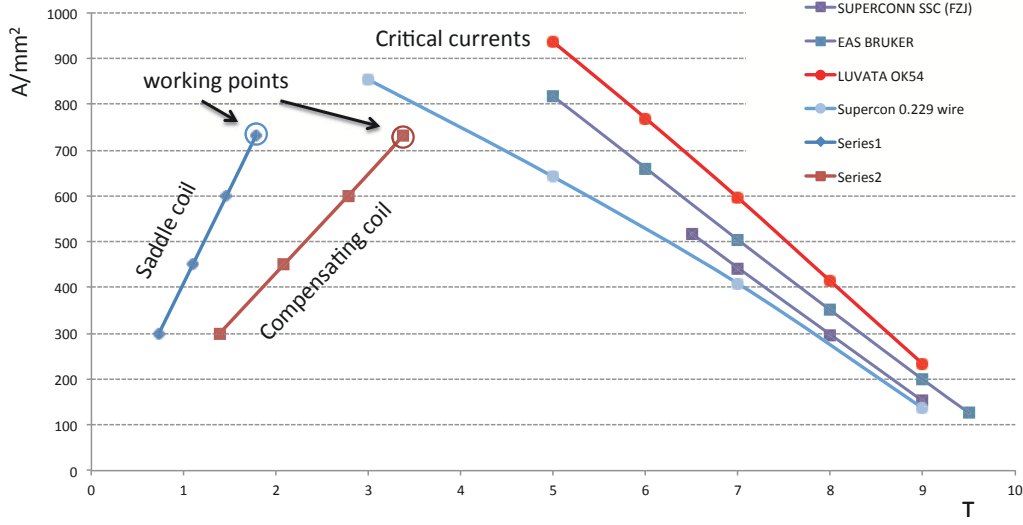


Figure 12: Load lines of the compensating (dark red) and saddle (dark blue) coils as compare to the critical current of the considered superconducting wires (see text). A realistic filling factor of 80% is considered for the superconducting coil wiring. The arrow indicates the working points.

#### 4.1.2 Target Polarization Measurements

The target polarization will be measured with an NMR system [114, 115, 116]. Polarimetry for nuclear targets has been studied extensively at BNL. The In-Beam-Cryostat that will hold HD targets within CLAS12 will have a short saddle coil to maintain transverse spin orientations. Keeping this coil short will both reduce the  $BdL$  deflection of electrons, as well as minimize spin diffusion from radiation damage (by changing the Larmor frequency across the target). However, the fields associated with this coil will be too non-uniform for NMR measurements. Instead, the central detector solenoid, able to provide a  $10^{-4}$  field uniformity within the target volume, will be used for NMR polarization monitoring. The target spins will readily follow the field as the HD-Ice magnetic system (compensating and saddle coils) is ramped down. NMR data will be collected after which the HD-Ice magnetic system will be ramped up. We anticipate a total cycle time of about 15 minutes (limited by how fast the fields can be changed without quenching the magnets), enabling NMR data to be collected several times a day. The systematic uncertainties in HD polarization are about 4% (relative). The largest single factor (contributing 2.8% relative) is the differential uncertainty on the gain of a lock-in amplifier whose scale must be changed by many orders of magnitude between equilibrium-polarization measurements and high-polarization frozen-spin measurements. Separation of signal and background in the calibration measurements contributes at the 1% level.

An additional estimate of the product of target and beam polarizations,  $P_B P_t$ , will be done also off-line by comparing the well known  $ep$  elastic asymmetry

$$A_{theo} = - \frac{\cos \theta_\gamma \sqrt{1 - \epsilon^2} + (\frac{Q^2}{4M^2})^{-\frac{1}{2}} \sqrt{2\epsilon(1 - \epsilon)} \sin \theta_\gamma \cos \phi_\gamma \frac{G_E}{G_M}}{\epsilon(\frac{Q^2}{4M^2})^{-1} (\frac{G_E}{G_M})^2 + 1} \quad (11)$$

with the measured asymmetry

$$A_{meas} = \frac{N^+ - N^-}{N^+ + N^-} = \frac{P_B P_t \sigma_{et}}{\sigma_0} \equiv P_B P_t A_{theo}. \quad (12)$$

For the ratio  $\frac{G_E}{G_M}$ , we will use values from polarization transfer measurements [117], which are expected theoretically to have the same (small) two-photon corrections as  $A_{LT}$  measurements. On average, the uncertainty in  $A_{LT}$  due to  $G_E/G_M$  will be about 2% (relative). The measurements will consist of measuring both an electron and a proton, and imposing missing momentum and energy cuts to isolate the elastic channel. Events from H and D will be distinguished through a multi-parameter fit to the missing mass and energy distributions. Fermi broadening in the deuteron generates peaks that are typically twice as wide as for hydrogen, for the conditions of this proposal. Due to this mixing, the errors will be approximately 1.4 times bigger than for targets which contain only H or D plus heavy materials such as nitrogen or aluminum.

The beam polarization will be measured periodically with the standard Hall-B Møller polarimeter.

### 4.1.3 The Impact of Møller Scattering

One of the main sources of background produced by a high-energy electron beam impinging upon a HD target is due to interactions of the electron beam with the atomic electrons (Møller scattering). This rate is several orders of magnitude larger than the inelastic hadronic production rate. A dedicated Monte Carlo study aimed at evaluating the impact of the Møller scattering on the detector occupancies has been performed using the CLAS12 GEANT4 based MC (gemc). The effect of HDice magnetic configuration on Møller electrons is depicted in Fig. 13, indicating an efficient screen of the background is feasible also with the transverse target magnet configuration.

The HD-Ice in-beam cryostat will be modified to optimize the target magnet configuration and achieve maximum uniformity for acceptable occupancies in the CLAS12 DC. The CLAS12 response to a single SIDIS event in gemc is shown in Fig. 14. The CLAS12 DC occupancies with the HD-Ice magnet configuration and a luminosity of  $5 \cdot 10^{33} \text{ cm}^{-2}\text{s}^{-1}$ , are below 2%, see Fig. 14. This is comparable (slightly worse) with the less than 1% occupancy achieved in the nominal CLAS12 configuration, corresponding to 5 T longitudinal field and  $10^{35} \text{ cm}^{-2}\text{s}^{-1}$ .

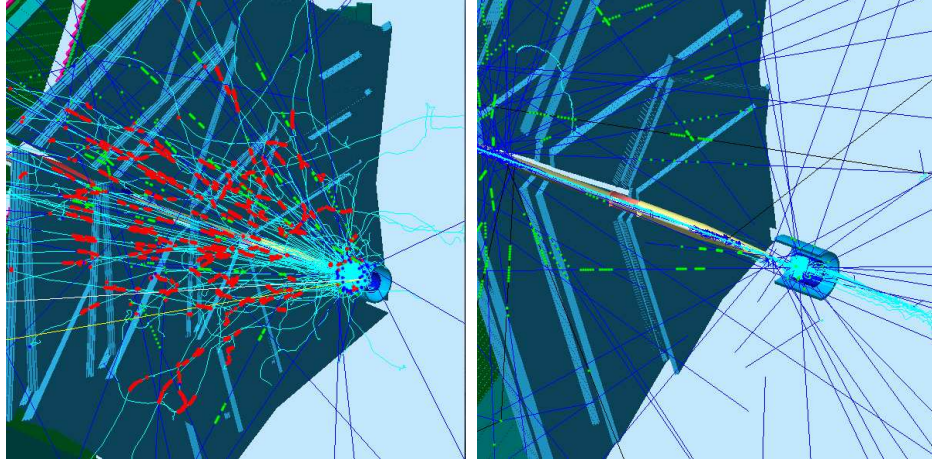


Figure 13: Comparison of the CLAS12 response without (left) and with (right) the magnetic field of the HDice magnet configuration. The blue lines are photons, the cyan are electrons.

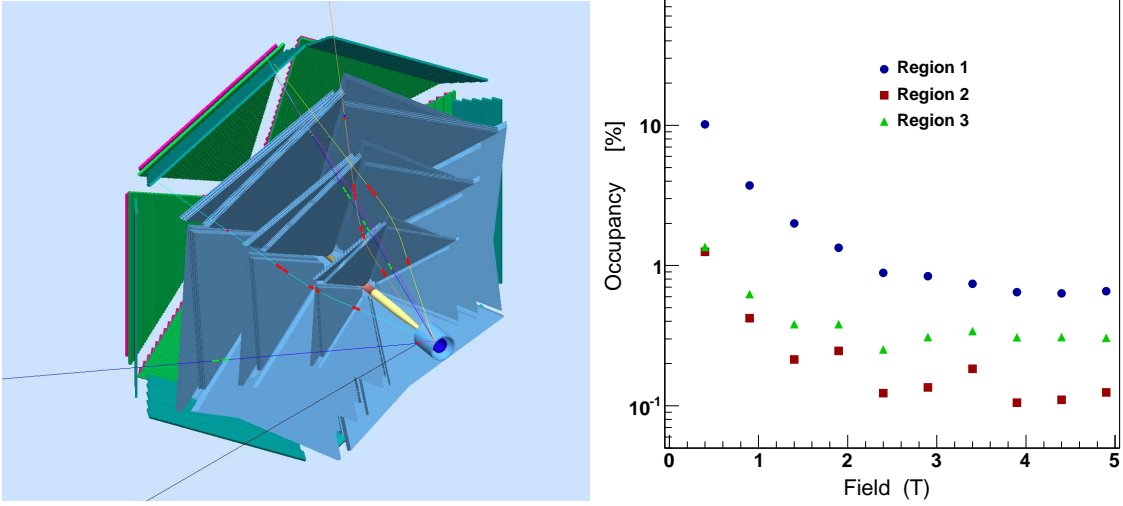


Figure 14: (Left) A SIDIS event in CLAS12 from gemc simulation. (Right) CLAS12 DC occupancies with the HD-Ice transverse magnetic system at  $5 \cdot 10^{33} \text{cm}^{-2} \text{s}^{-1}$ , as a function of the central solenoid field strength. The foreseen working point is at 2 T.

#### 4.1.4 The CLAS12 Particle Identification

The proposed experiment will use the upgraded CLAS12 spectrometer with the low threshold Cherenkov counter replaced by a RICH detector in (at least) two sectors.

In the baseline design of CLAS12, particle identification (PID) in the forward detector is obtained by using the high threshold Cherenkov counter (HTCC), the low threshold Cherenkov counter (LTCC) and the Time-of-flight scintillator arrays (TOF) (see Fig. 15). In the  $\sim 2.5 - 5$  GeV/c momentum region, the  $\pi/K$  separation relies only on the LTCC performance. Moreover, in the  $4.7 - 8$  GeV/c momentum region it is not possible to separate protons from kaons. In general, this PID system matches the requirements of the physics program at 12 GeV. However there are some physics reactions of high interest, such as the one covered by this proposal, that cannot be accessed without a better PID, especially for charged kaon detection. For semi-inclusive processes at 12 GeV beam energy, the  $K/\pi$  ratio is of the order of  $10 - 15\%$ , see Fig. 16, thus the required rejection factor for pions is around  $1 : 1000$ , corresponding to greater than  $4\sigma$  pion-kaon separation, where  $\sigma$  is the Cherenkov angle resolution. With the present configuration, assuming a realistic pion detection inefficiency for the LTCC of  $10\%$ , the  $\pi/K$  contamination is  $1 : 1$ . A RICH detector, to be installed in place of the low threshold Cherenkov counter, will significantly improve the CLAS12 particle identification overcoming the above limitations without having any impact on the baseline design of CLAS12.



Figure 15: Hadron particle identification in CLAS12.

#### 4.1.5 The CLAS12 RICH detector

To fit the CLAS12 geometry, the RICH should have a projective geometry with six sectors matching the torus bores and covering scattering angles from  $3^\circ$  to  $30^\circ$  (see Fig. 17). Being downstream to the torus magnet at more than 5 m from the interaction point, the RICH has to cover a large surface, each sector having an area

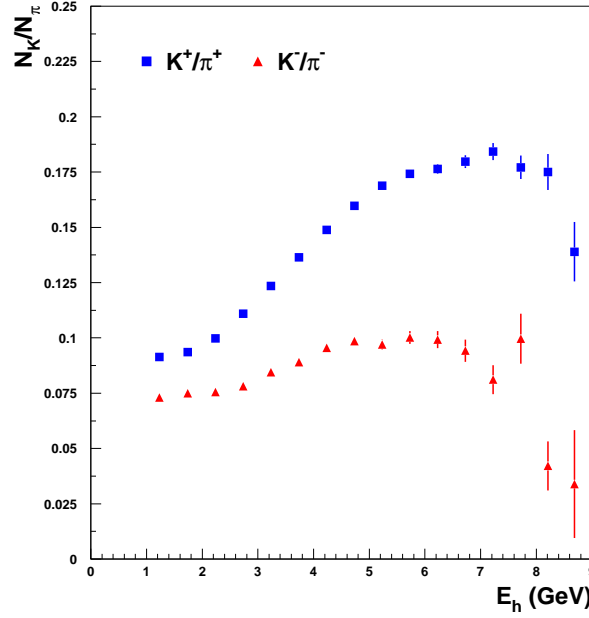


Figure 16: Semi-Inclusive kaon versus pion yield ratio.

of the order of 4 m<sup>2</sup> in the front and 8 m<sup>2</sup> in the back. The RICH total thickness cannot exceed 1 m, being the detector constrained between existing equipments. The proposed solution is based on the concept of the proximity focusing RICH, with a mirror system mainly devoted to reduce the photon detector area. In the momentum range of interest an aerogel RICH represents the best solution for the identification of  $\pi/K/p$  as shown in Fig. 18. This implies detecting Cherenkov light in the visible wavelength range and using photomultipliers (PMTs) as photon detectors. Ongoing Monte Carlo studies (see next section) show that the wanted pion-kaon separation at 8 GeV/c momentum can be achieved if the detector pad size is less than 1x1 cm<sup>2</sup>, thus the use of Multi-Anode PMTs is anticipated.

The use of aerogel as radiator and the detection of light in the visible wavelength range is an expensive solution. Work is in progress to limit the area of the photon detector to about 1 m<sup>2</sup> per sector. Studies of the spatial distributions of the Cherenkov photons impact point at the detection surface show that high-momentum particles concentrate in a limited forward region close to the beam line (see Fig. 19).

The approach is, thus, to instrument a limited area around the beam line to have direct detection in the forward region at high momenta, while at large angles and lower momenta a system of focusing mirrors catches the light and focalize it onto the photon detector. A drawing of the proposed solution is illustrated in Fig. 20, where the main components of the systems are shown: the planar mirror (positioned before

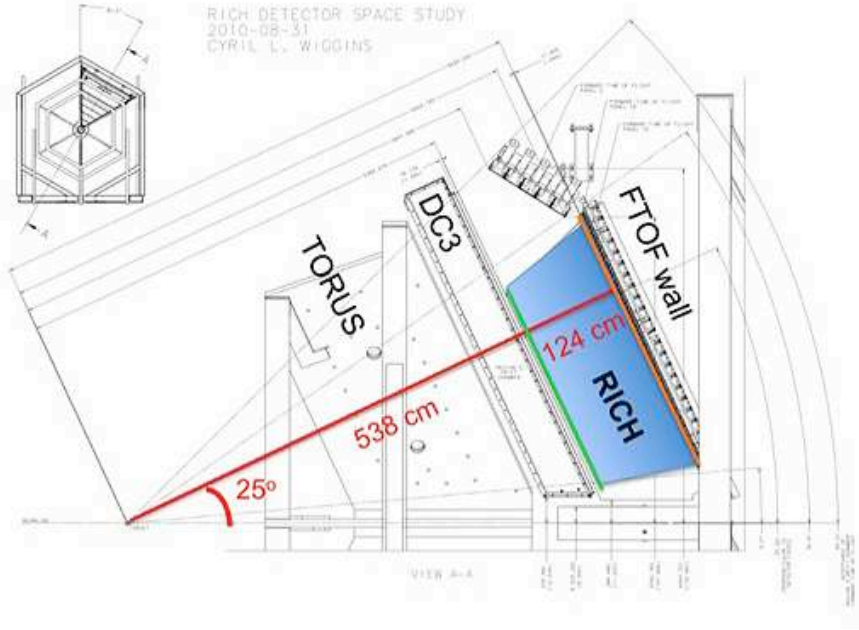


Figure 17: RICH detector space and position in the CLAS12 spectrometer.

the radiator), the aerogel radiator, the proximity gap, the PMTs plane covering the angular region between  $3^\circ$  and  $14^\circ$ , and the elliptical mirror which reflects the light produced by the particles emitted at angles larger than  $14^\circ$  towards the planar mirror.

Preliminary Monte Carlo studies based on GEANT4 with a realistic geometry of the CLAS12 detector and events generated with PYTHIA have been performed with the aim to optimize all the components of the detector. The dimensions of the radiator thickness and the gap length as well as the pad/pixel size of the photon detector have been varied in order to find the optimal combination which gives the smallest reconstruction error in the Cherenkov angle and the highest number of photoelectrons. An average number of 10 and 5 photoelectrons per ring has been obtained for the direct and reflected light collection, respectively. An example of simulated events in the proposed RICH geometry is shown in Fig. 21, where both direct and reflected Cherenkov photons are detected by the PMTs.

In order to have a precise information about the RICH performances in terms of pion/kaon separation, a pattern recognition algorithm based on the event-wise Direct Ray Tracing (DRT) technique has been implemented. For each hypothesis of particle type(s), given the track(s) information, DRT realistically estimates the produced photon hits pattern to be compared with the measured one by means of a likelihood function. The most probable hypothesis of particle types(s) is assumed to be the true one. As a particle identification goodness estimator ( $R_{QP}$ ) one minus the

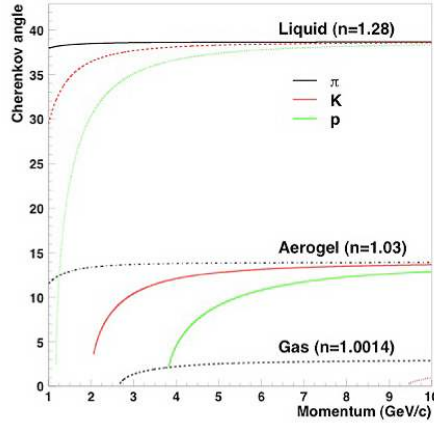


Figure 18: Cherenkov angle versus particle momenta for  $\pi$ ,  $K$ ,  $p$  and different radiators.

ratio of the second most probable over the most probable hypothesis is taken.

The results for high-momentum particles, obtained using the RICH configuration shown in Fig. 20 with aerogel of increasing thickness from 2 to 6 cm, a gap length of  $\sim 100$  cm and a pad size of 0.6 cm, are shown in Fig. 22. The simulation accounts for all the relevant optical effects, like the mirror reflectivity, the aerogel photon absorption and Rayleigh scattering. In the figure the goodness parameter  $R_{QP}$  for the different particles identifications is shown. As it can be seen, the contamination is widely smaller than 1%, i.e. the probability that a pion is misidentified as a kaon in the most challenging momentum range (6-8 GeV/c) is 0.5%.

The preliminary Monte Carlo results on the performances of the proposed RICH are encouraging. The project presents some critical points, some of which have been already addressed in 2011 with laboratory tests of the components. In addition, a test of a preliminary prototype has been performed in summer 2011 using the hadron beam of the T9 line at CERN. The prototype was composed by an aerogel radiator of different thicknesses and eight multi-anode H8500 photomultipliers by Hamamatsu,  $5 \times 5$  cm<sup>2</sup> devices with a  $8 \times 8$  matrix of 6 mm pixels (see Fig. 23). The good capabilities of those PMTs as single photon detector have been verified both with a low intensity laser beam and during the hadron beam test. The left plot of Fig. 24 shows a single photon spectrum measured during the CERN tests. We see a clear Cherenkov peak, well separated from the pedestal. Rough estimate of the single photon detection efficiency has been measured with the laser tests to be at least 80%. The Cherenkov rings produced by the high energy pions have been clearly measured, as shown in the right plot of Fig. 24. These results are very promising and have been used to validate the GEANT4 simulation of the final detector. A new prototype, with dimensions and geometry closer to those of the final detector, is under construction and will be tested in summer 2012 both with the electron beam of the Beam Test

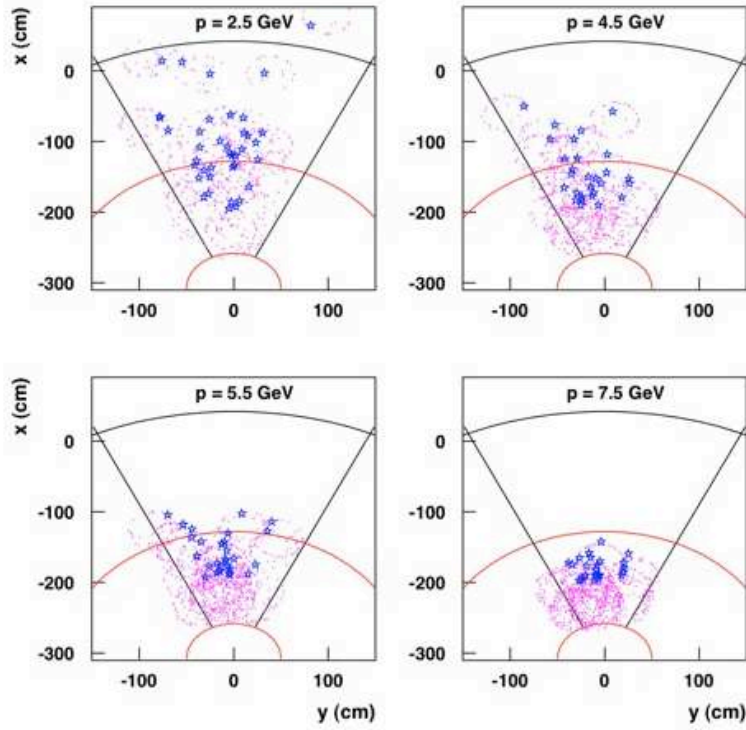


Figure 19: Spatial distributions of the particle impact point at the RICH entrance (stars) and gamma impact point at the detector surface (dots) for few overlapped events. The plots distinguish among particle of increasing average momentum, from 2.5 GeV/c up to 7.5 GeV/c, from top to bottom and left to right. High-momentum particles concentrate in a limited forward region close to the beam line, arbitrarily delimited by the two dashed lines just for an illustration purpose.

Facility in INFN Frascati National Laboratory and with the CERN-T9 hadron beam.

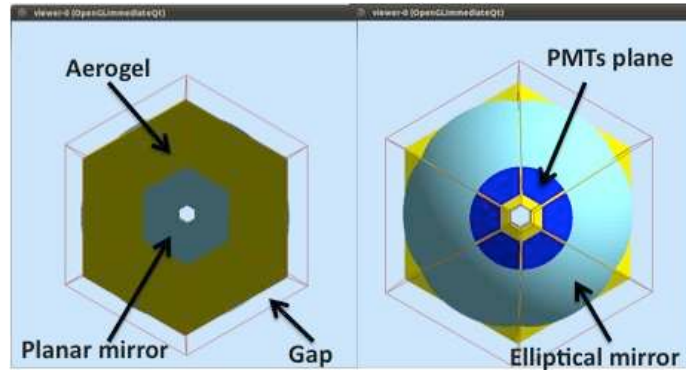


Figure 20: Drawing of the proposed proximity focusing RICH with focusing mirrors.

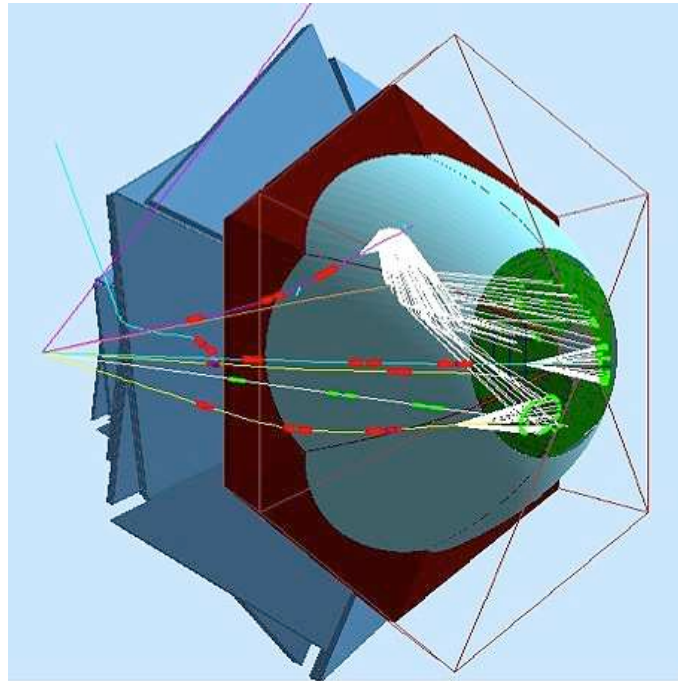


Figure 21: Example of events simulated with GEANT4

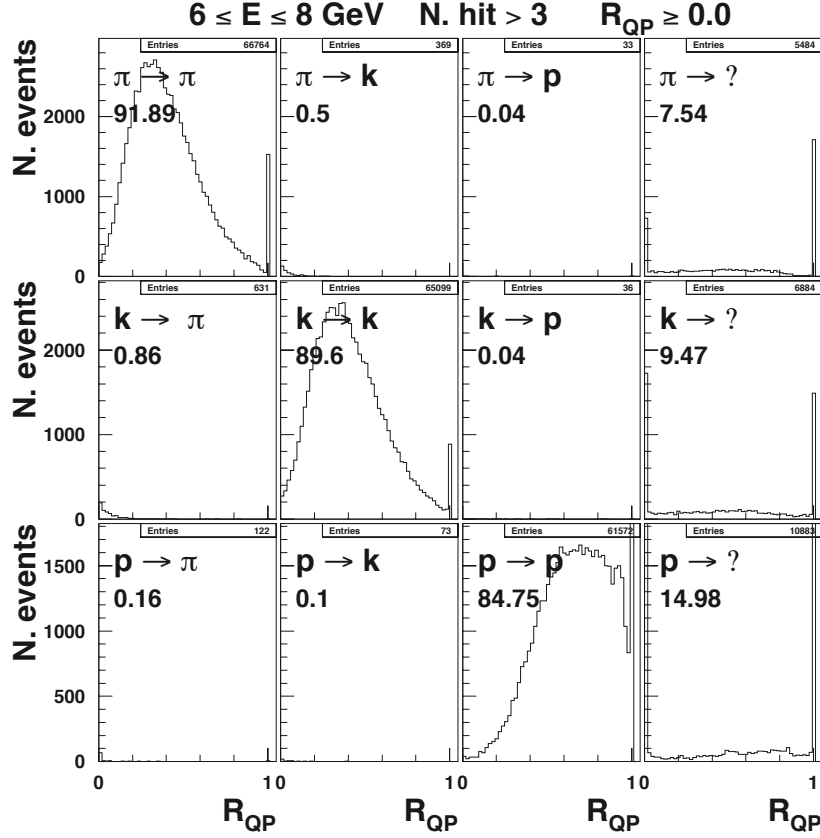


Figure 22: Goodness parameter  $R_{QP}$  distribution for the different particles hypothesis in the most challenging momentum range between 6 and 8 GeV/c. The rows correspond to true particle types, from pion (top) to proton (bottom). The columns correspond to identified particle types, from pion (left) to unidentified (right). The diagonal elements give the identification efficiency, and the off-diagonal the contamination, when a minimum of 4 detected photon hits is required. In the simulation, all the relevant optical effects, i.e. mirror reflection efficiency, aerogel absorption and Rayleigh scattering are taken into account.



Figure 23: The photo-detection area of the RICH prototype used at the test beam at CERN.

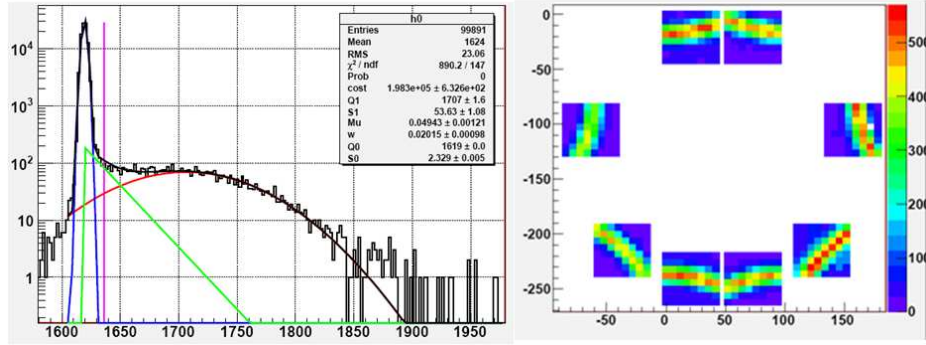


Figure 24: (left) Single photon spectrum for one H8500 channel measured at CERN (pink vertical line represent the pedestal cut); (right) Example of Cherenkov rings for pions with 10 GeV/c momentum, measured with eight H8500 photomultipliers.

## 4.2 The Measurement

### 4.2.1 Event Reconstruction

Final-state hadrons and the scattered electron will be detected by the CLAS12 spectrometer. The HD-Ice and its magnet configuration have been implemented in the GEANT4 simulation of CLAS12 to study the reconstruction efficiencies and resolutions in the presence of the transverse field of the HD-Ice target.

The corresponding resolutions for charged particles, which are the main concern, are shown in Figs. 25, 26. The resolution on the forward electron track meets the specification of the CLAS12 technical design report, except for the angle measurement at low momentum. The reconstruction of the large-angle proton track is worse but not far from the resolutions in momentum and polar angle achievable with nominal CLAS12 configuration, which are 6% and 7 mrad, respectively. The proton angular resolution is limited by the straggling in the HD-ice magnet coils especially at low momenta, whereas its momentum resolution is limited at large momenta by the reduced field of the central detector solenoid. These preliminary studies were performed with an oversimplified description of the HD-Ice magnetic system and in-beam cryostat, resulting in a substantial overestimation of the material budget effect. A more realistic geometry is under study.

### 4.2.2 Event Identification

Final-state hadrons and the scattered electron will be detected by the CLAS12 spectrometer. Electrons are separated from hadrons using Cherenkov counters and electromagnetic calorimeters. Pions will be identified using Cherenkov counters and measurement of time of flight. The use of the CLAS12 RICH detector would ensure pion/kaon separation in a wide momentum range (up to approximately 8  $GeV/c$ ). Pion and kaon momenta will be reconstructed in the CLAS12 drift chamber system, embedded within the toroidal magnetic field. For the proposed experiment, gammas from  $\pi^0$  decays (or from  $\eta$  decays) will be reconstructed using the forward angle electromagnetic calorimeter (FC) and the new preshower calorimeter (PCAL). Kinematic distributions of electrons and final state hadrons are shown in Fig. 27 and Fig. 28.

Figure 29 shows the correlation of some relevant kinematic variables with the scattering angle. Electron detection at large angles (larger than 20 degrees) is mandatory to explore the large  $Q^2$  regime, whereas hadron identification is required in the middle angle range (15-20 degrees) to reach large  $P_{h\perp}$  values. The CLAS12 forward detector is perfectly suitable for such measurements since designed to cover angles up to 40 degrees.

### 4.2.3 Acceptance and Data Analysis

Although SSAs are typically not too sensitive to acceptance corrections, in the case of the transverse target, due to the large number of contributions appearing as different

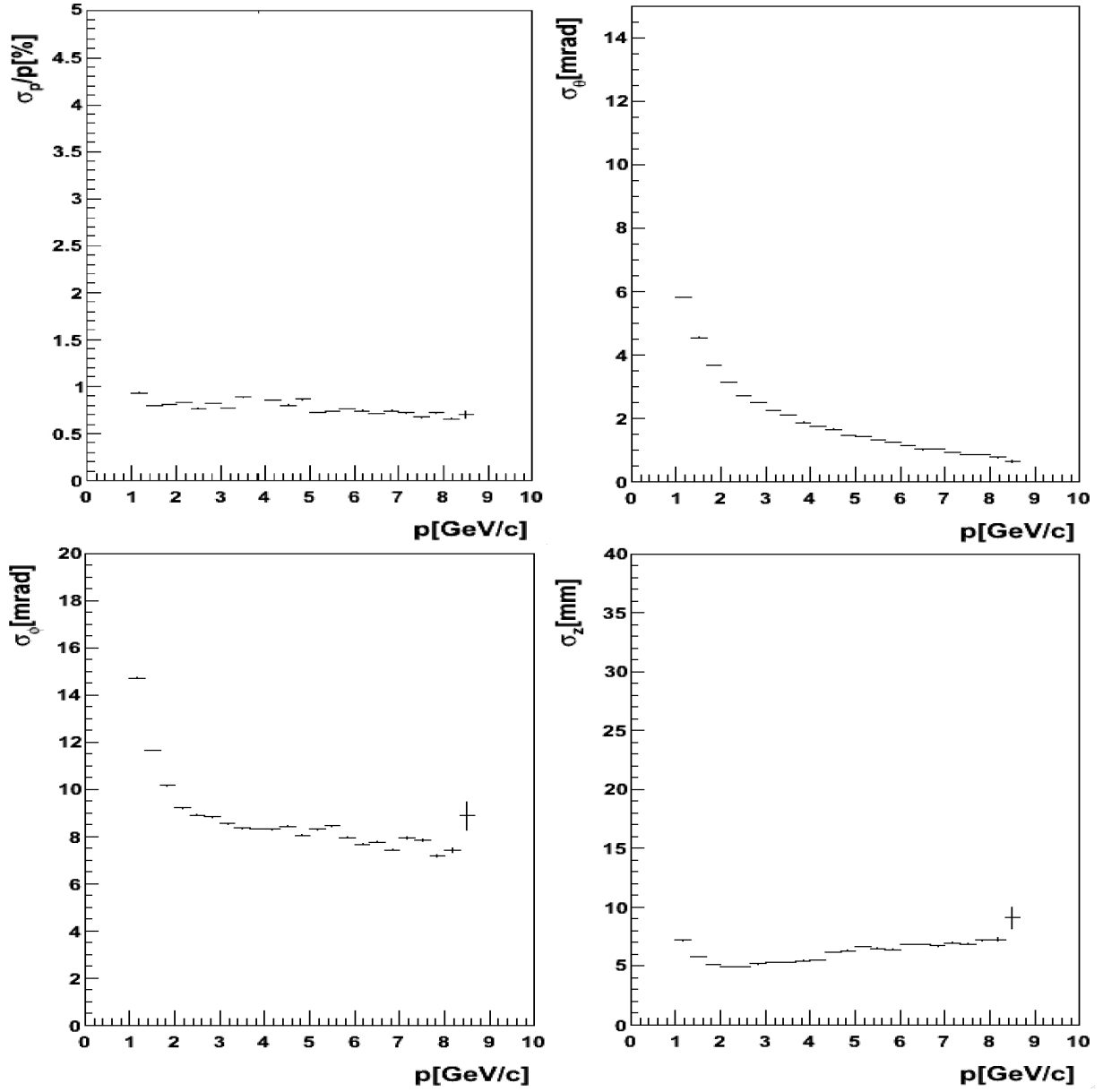


Figure 25: Resolutions in momentum, polar angle, azimuthal angle and reconstructed vertex for forward charged tracks (electrons) from the CLAS12 reconstruction program. Reconstruction of events was performed using a GEANT4 simulation accounting for the HD-Ice configuration and transverse field of the target.

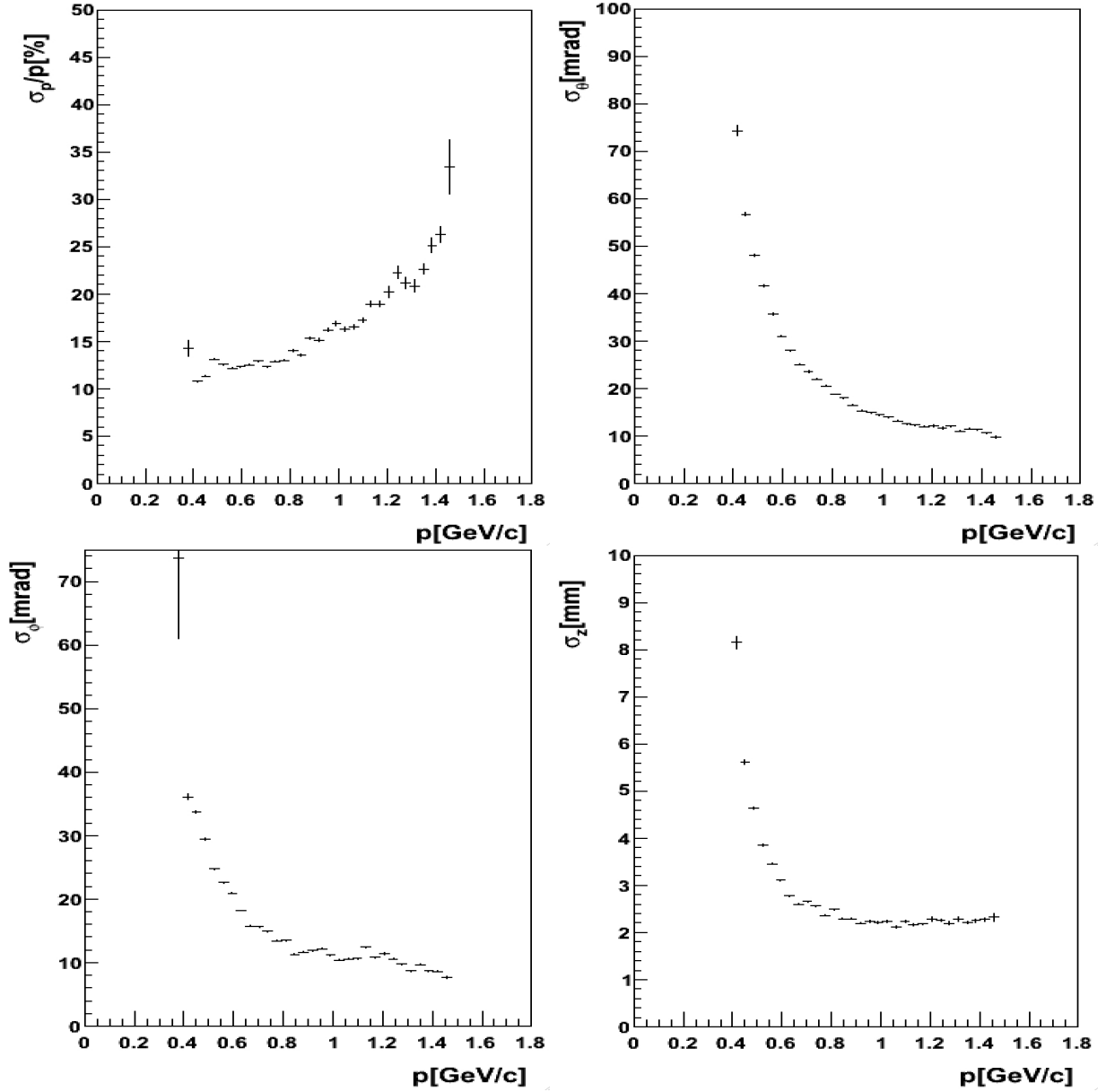


Figure 26: Resolutions in momentum, polar angle, azimuthal angle and reconstructed vertex for large angle charged tracks (protons) from the CLAS12 reconstruction program. Reconstruction of events was performed using a GEANT4 simulation accounting for the HD-Ice configuration and transverse field of the target.

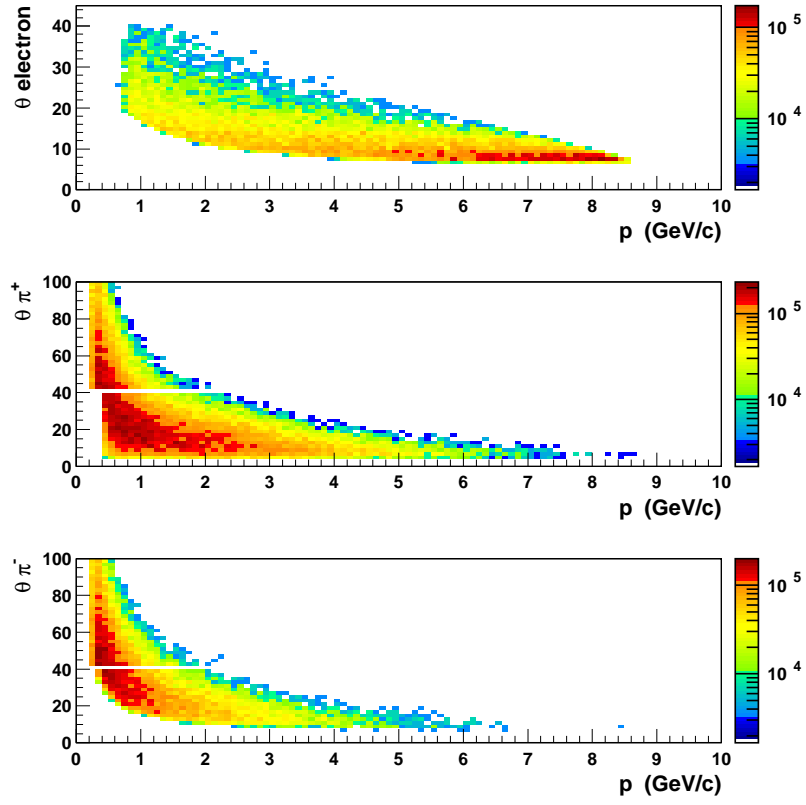


Figure 27: Kinematic distributions of electrons and final state hadrons.

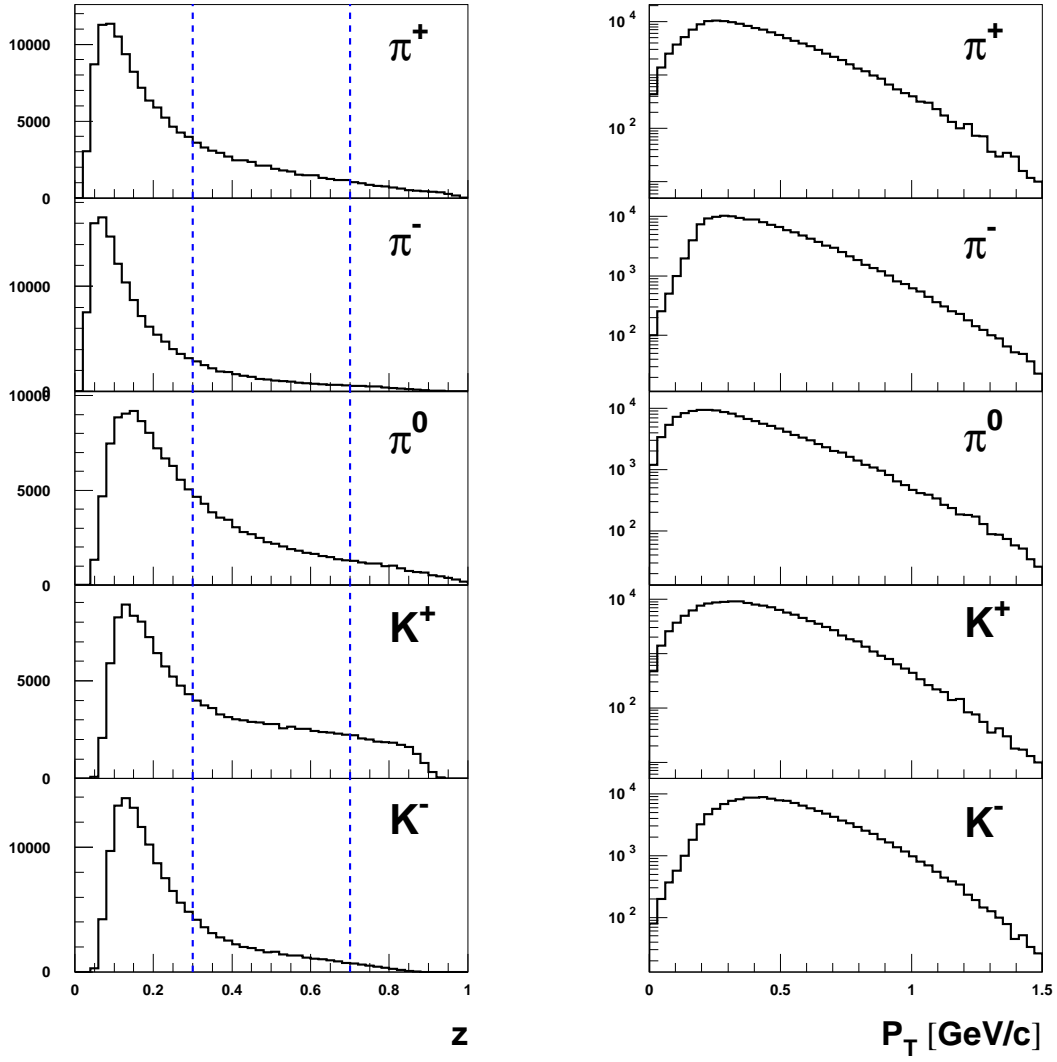


Figure 28: Typical kinematic distributions of CLAS12 SIDIS hadrons with transverse target. The dashed lines define the  $z$  region selected for SIDIS.

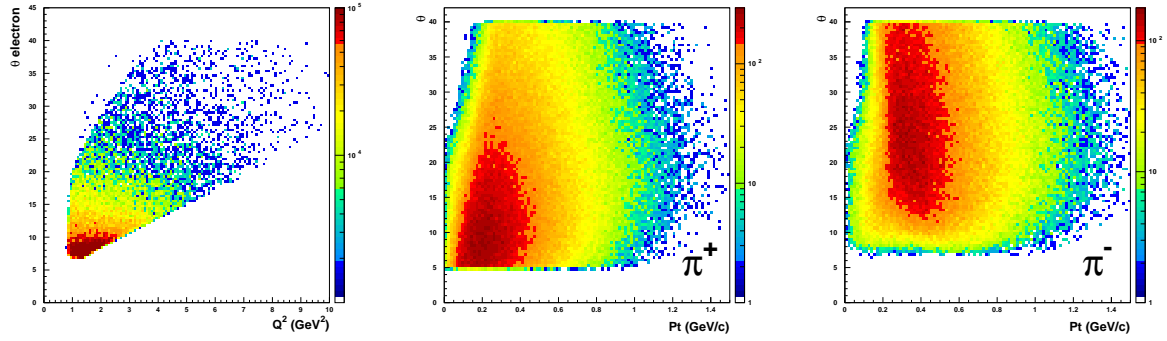


Figure 29: Kinematic coverage of CLAS12 SIDIS hadrons with transverse target.

azimuthal moments in the cross section, the acceptance corrections are more important. The analysis of the transverse target data requires fits in the 2-dimensional space of the relevant azimuthal angles  $\phi$  and  $\phi_S$ . A detailed procedure on the accounting for acceptance corrections in the separation of the different azimuthal moments was developed by the HERMES collaboration [83]. According to this method, a fully-differential (thus virtually free from acceptance effects) parametrization of the asymmetries is extracted from the data itself with a fully-unbinned maximum likelihood fit. The parameterization is then used in input to an originally unpolarized Monte Carlo simulation which accounts for a complete model of the instrumental effects (acceptance, smearing, inefficiencies...) to generate a pseudo-data sample. The systematics effects are evaluated as the difference of the asymmetries extracted from the pseudo-data sample and the parameterization in input to the Monte Carlo. A similar procedure has been applied to estimate the expected acceptance corrections for e.g. the Sivers asymmetries as extracted in the CLAS12 acceptance. In this case, a parametrization based on a phenomenological model for the Sivers function [43] was used. This parametrization, tuned to the HERMES and COMPASS data, was evaluated extrapolated to the CLAS12 kinematic domain.

#### 4.2.4 Count Rates and Statistical Errors

With the proposed configuration as described in Section 4.1, a luminosity of  $5 \cdot 10^{33} \text{ cm}^{-2}\text{s}^{-1}$  is expected. The yields of SIDIS pions and kaons are estimated using a Monte Carlo simulation of the acceptance and smearing of the detector, based on the PYTHIA generator tuned to the multiplicities measured at the HERMES experiment. The statistics of the proposed experiment is calculated for 100 days of data-taking (i.e. for the total requested beam time, 110 days, diminished by a 10% duty-factor accounting for calibration runs, empty target runs, and supportive tests). The expected number of SIDIS pions and kaons within the kinematic limits:  $Q^2 > 1 \text{ GeV}^2$  (corresponding to  $x > 0.05$ ),  $W^2 > 4 \text{ GeV}^2$ ,  $0.10 < y < 0.85$  and  $0.3 < z < 0.7$  are:

17.6 M, 5.8 M and 3.9 M for  $\pi^+$ ,  $\pi^-$ , and  $\pi^0$ , respectively, and 1.9 M and 0.4 M for  $K^+$  and  $K^-$ , respectively. A squared missing mass greater than  $2 \text{ GeV}^2$  was required to suppress the contamination from exclusive channels. The  $\pi^0$  yields were obtained selecting the range  $0.097 < m_{\gamma\gamma} < 0.179 \text{ GeV}/c^2$  of the  $2\gamma$  invariant mass spectrum, corresponding to  $\pm 2\sigma$  from the mean value ( $\langle m_{\gamma\gamma} \rangle = 0.138 \text{ GeV}/c^2$ ).

The hydrogen target polarization is assumed to be 60%, whereas a beam polarization of 85% is predicted. The dilution factor for the hydrogen target is of the order of  $1/3$ . All the above factors have been taken into account when calculating the statistical uncertainties on the asymmetries (see Section 4.3). The number of days was chosen to achieve a statistical error that is not significantly larger than the systematical error at the highest  $x$  and  $P_{h\perp}$  points.

#### 4.2.5 Systematic Errors

The systematic uncertainties can be divided into two categories: those that scale with the measured asymmetry and those that are independent of the measured results. In the first category, the dominant uncertainty is expected to be that from the target polarization and the dilution from the target material other than HD, see Table 3. For the second category, we have taken our best estimate of the magnitude of the systematic effect, and divided by the average expected proton asymmetry.

One of the main contributions to the estimated relative uncertainties, summarized in Table 5, comes from the procedure used to separate the azimuthal moments of interest from other, potentially non-zero, azimuthal asymmetries (for example a twist-3  $\sin(\phi_S)$  moment). Another large contribution is from possible contamination of the SIDIS pion event sample by pions from decays of diffractive vector mesons, mainly  $\rho^0$  (the contamination for kaons is expected to be much smaller). Thanks to the large acceptance of CLAS12, the asymmetries from background processes, such as  $\rho^0$  production, will be measured simultaneously and can thus be corrected for, as the size of the contamination can be measured as well. Moreover also the SIDIS vector meson asymmetries can be studied, and are the matter of the di-hadron proposal also presented to PAC39. Based on our previous studies for the EG1, e1f and e16 experiments, the uncertainty from radiative corrections will be a minor contribution.

We conservatively estimate the average total relative systematic error on the proton SSAs to be of order 7%, sufficiently small for a very significant measurement.

| Error source               | Systematic error (%) |
|----------------------------|----------------------|
| D background               | 4                    |
| Target polarization $P_T$  | 4                    |
| Acceptance corrections     | 4                    |
| Al background contribution | 3                    |
| Radiative corrections      | 2                    |
| Total                      | $\sim 7$             |

Table 5: Estimated contributions to the relative systematic uncertainty on the proton TTSA's in SIDIS.

### 4.3 Projected Results

The projected CLAS12 statistical precision on the  $A_{UT}$  TTSA asymmetries for pions and charged kaons on a proton target, corresponding to 100 days of data-taking with the HD-Ice target, are shown in Figs. 30-33. The kinematic region considered for these projections is the following:  $Q^2 > 1 \text{ GeV}^2$  (corresponding to  $x > 0.05$ ),  $W^2 > 4 \text{ GeV}^2$ ,  $0.10 < y < 0.85$  and  $0.3 < z < 0.7$ . A squared missing mass greater than  $2 \text{ GeV}^2$  was also required. In particular, the  $\pi^0$  yields were obtained selecting the range  $0.097 < m_{\gamma\gamma} < 0.179 \text{ GeV}/c^2$  of the  $2\gamma$  invariant mass spectrum, corresponding to  $\pm 2\sigma$  from the mean value ( $\langle m_{\gamma\gamma} \rangle = 0.138 \text{ GeV}/c^2$ ). The projected results were obtained from a Monte Carlo simulation including a description of the CLAS12 geometry as well as detector acceptance and smearing effects. QED radiative effects were neglected since known, from previous studies, to be small. Here, a target polarization of 60% and a dilution factor of 1/3 were assumed.

Figure 30 shows the CLAS12 1-dimensional projected results for the Collins amplitudes as a function of  $x$ ,  $z$ , or  $P_T$ . In most of the bins the projected error bars (statistical uncertainties) are not visible since they are smaller than the dots size. The comparison between the projected results for CLAS12 and the HERMES results [83], also reported in the figure, shows the remarkable improvement expected for CLAS12 in terms of statistical precision and kinematic coverage, especially in the valence region (intermediate-to-high  $x$ ) and in the high- $P_T$  region. A similar plot is shown in Fig. 31 for the Sivers amplitudes. Here the projected results (based on a Monte Carlo simulation) were modulated using a parametrization based on a phenomenological model for the Sivers function [43]. The projected results show sizable Sivers amplitudes for pions and kaons. However, the magnitude of the projected amplitudes is purely indicative, as it results from an extrapolation of the parametrization, tuned to the HERMES and COMPASS data, to the CLAS12 kinematic domain. The use of this parametrization also allowed to estimate the global systematic uncertainties due to acceptance and detector smearing effects, also shown in the figure, based on the procedure described in Section 4.2.3.

In Figs. 34-35, projected results are shown for 2-dimensional extractions of the Sivers amplitudes in bins of  $P_T$  as a function of  $x$ , and in bins of  $x$  as a function of  $P_T$ , respectively.

Measurements of amplitudes for identified pions and kaons will provide precious information not only on the contribution to the distribution functions involved from the various quark flavors (e.g., it would allow for constraints on the contribution from the strange sea quarks), but also on the ratio of favored to unfavored polarized fragmentation functions, complementary to  $e^+e^-$  data.

Thanks to the high statistics achievable in 100 days of measurements, a 4-dimensional analysis of the extracted azimuthal moments can be performed. This allows the disentanglement of all the specific kinematic dependences and a deeper inspection of the mechanisms generating the asymmetries. The projected statistical precision for a 4-dimensional analysis of the  $A_{UT}$  TTSA amplitudes are reported for  $\pi^+$  and  $K^+$  in

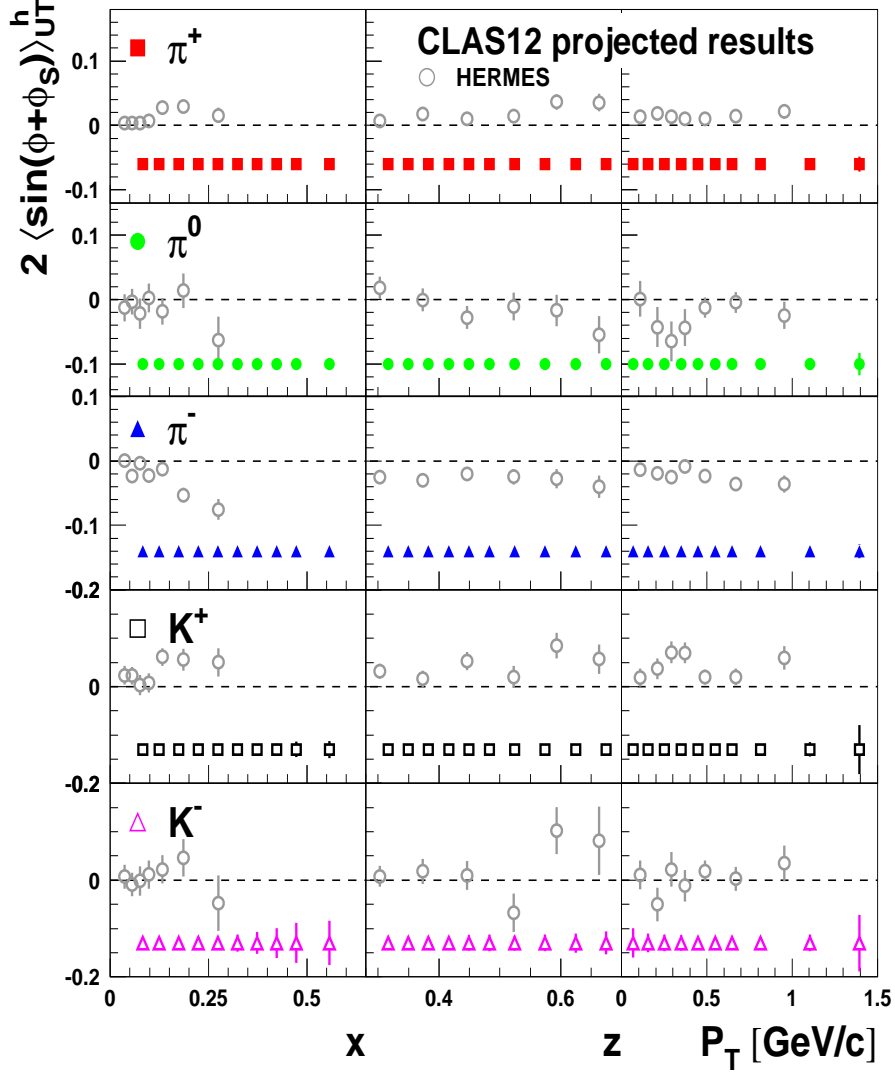


Figure 30: Expected statistical uncertainties for the Collins amplitudes as a function of  $x$ ,  $z$  and  $P_T$ . Overlaid are also shown the corresponding HERMES results.

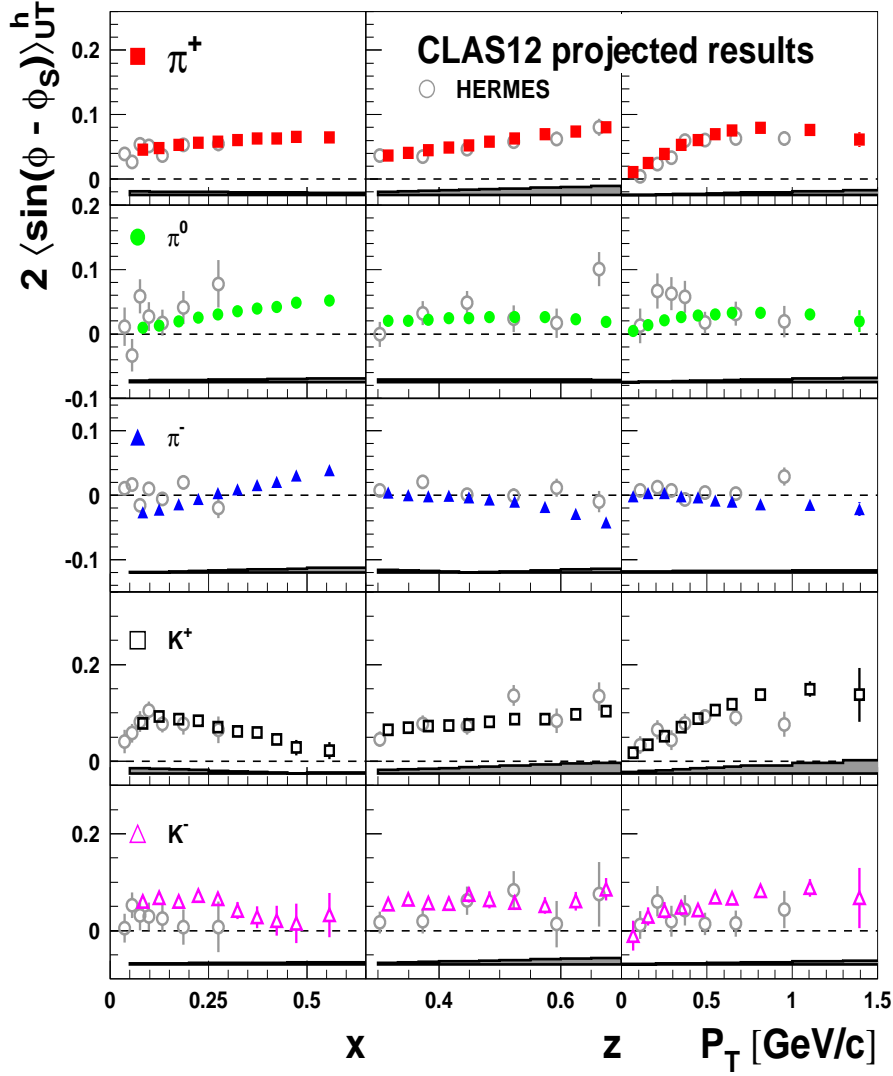


Figure 31: Projections for the Sivers amplitudes as a function of  $x$ ,  $z$  and  $P_T$ . Overlaid are also shown the corresponding HERMES results. The projected amplitudes were obtained by modulating the Monte Carlo data with a parametrization based on a phenomenological model for the Sivers function [43]. Estimates of the expected systematic uncertainties (global acceptance and detector smearing effects) are also shown.

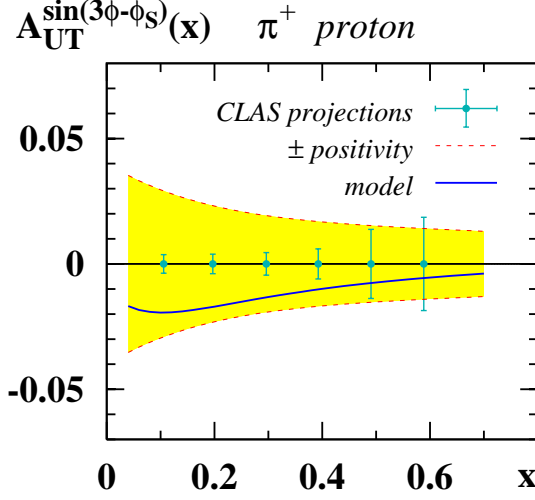


Figure 32: The  $A_{UT}^{\sin(3\phi-\phi_s)}$  asymmetry in  $\pi^+$  electro-production from proton target in the kinematics of CLAS12 as function of  $x$  [63] for a bin in  $P_T$  ( $0.45 < P_T < 0.6$ ). Solid curve presents the prediction of relativistic covariant model [118]. The shaded area is the region allowed by positivity.

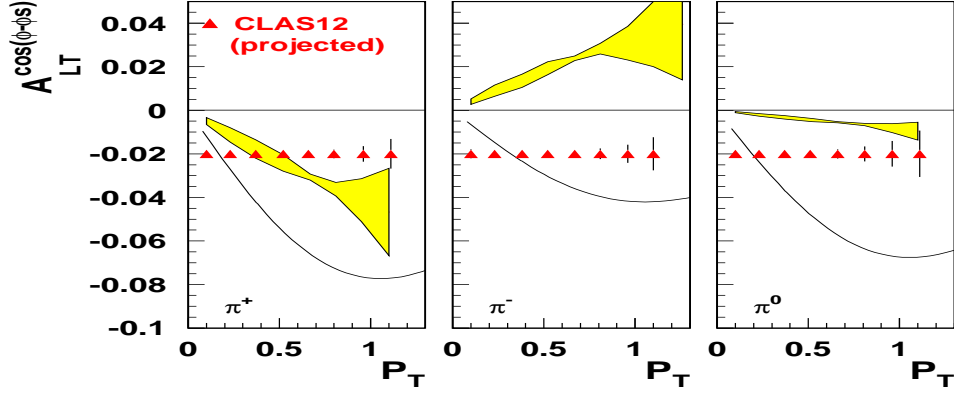


Figure 33: Expected statistical uncertainties for the  $A_{LT}^{\cos(\phi-\phi_s)}$  amplitudes sensitive to the  $g_{1T}^\perp$  TMD as a function of  $x$ . Overlaid are also a band from calculations [119] of  $g_{1T}$  based on two transverse-momentum Gaussian widths ( $\langle k_T^2 \rangle = 0.15$  and  $0.25$   $\text{GeV}^2$ ). The curve is from light-cone constituent quark model [69].

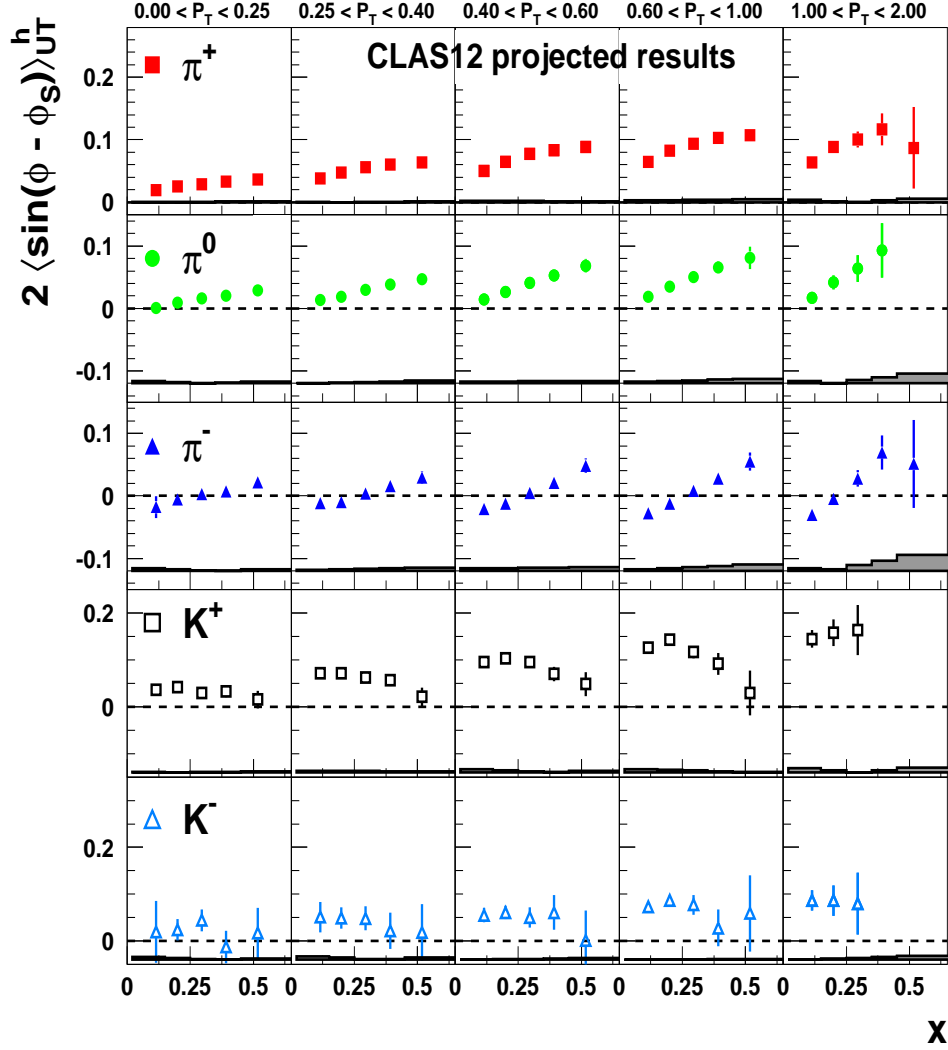


Figure 34: Two-dimensional projections for the Sivers amplitudes (based on the use of a phenomenological model for the Sivers function [43]). Bins in  $P_T$  as a function of  $x$ . Estimates of the expected systematic uncertainties (global acceptance and detector smearing effects) are also shown.

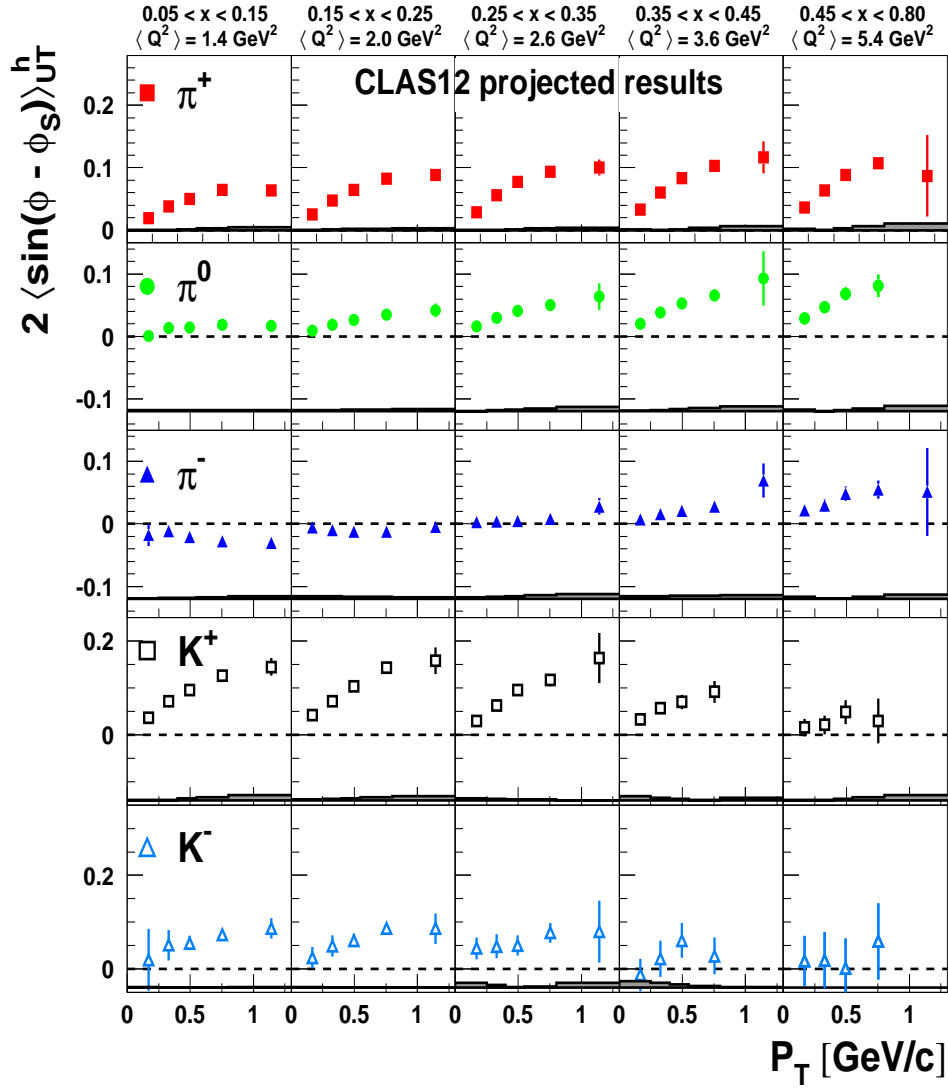


Figure 35: Expected 2-dimensional projections for the Sivers amplitudes (based on the use of a phenomenological model for the Sivers function [43]). Bins in  $x$  as a function of  $P_T$ . Estimates of the expected systematic uncertainties (global acceptance and detector smearing effects) are also shown.

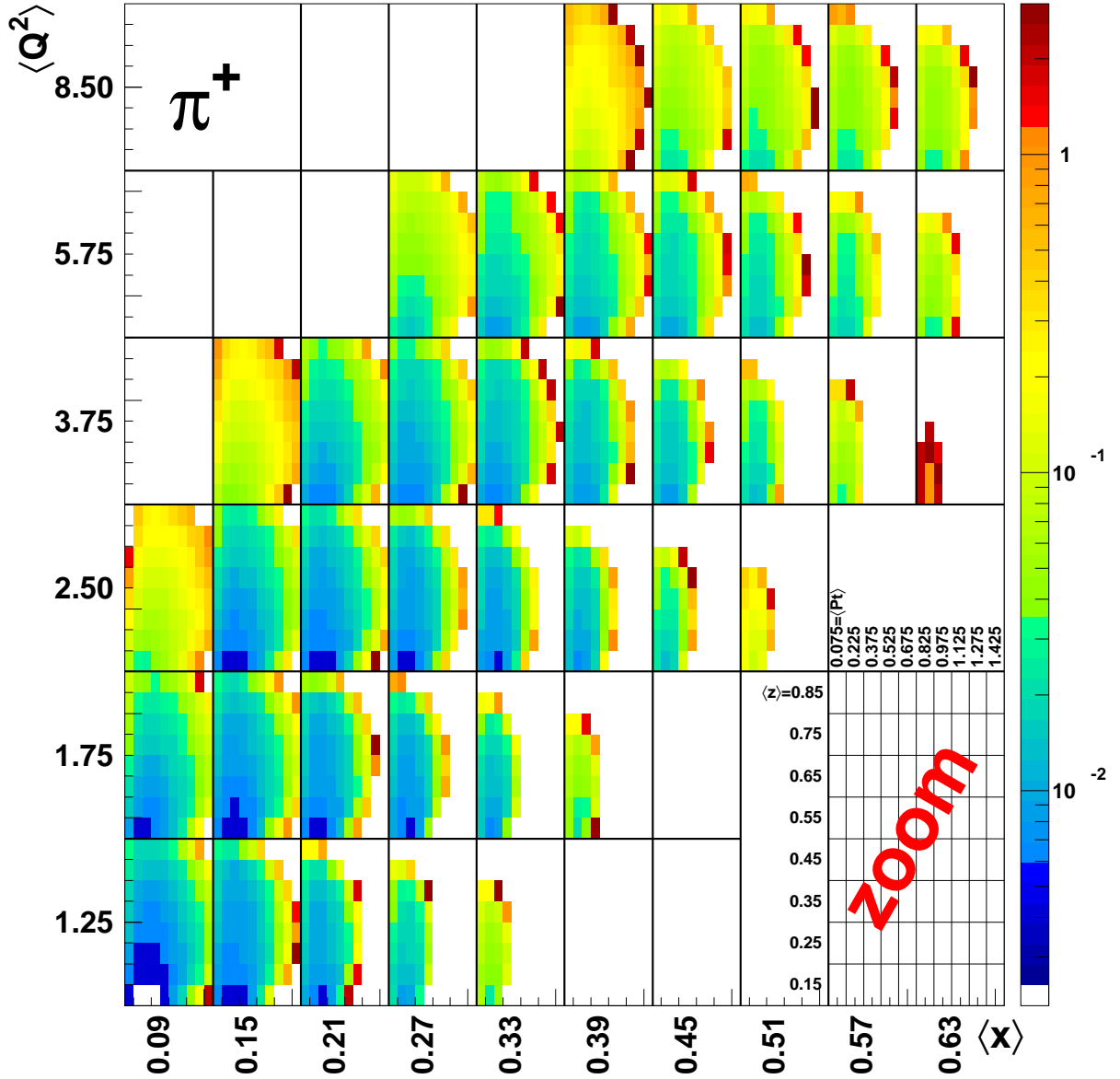


Figure 36: Expected statistical errors in a 4-dimensional analysis of  $A_{UT}$  TTSAs for  $\pi^+$ . Each  $x$ - $Q^2$  bin is subdivided in a matrix of  $z - P_T$  bins, as depicted in the bottom-right corner. For each bin the average kinematical values are reported. The colors correspond to the statistical errors that can be achieved in 100 days of data-taking. Note a precision of few percents can be obtained even in the high- $Q^2$  bins for  $P_T$  values up to 1 GeV/c.

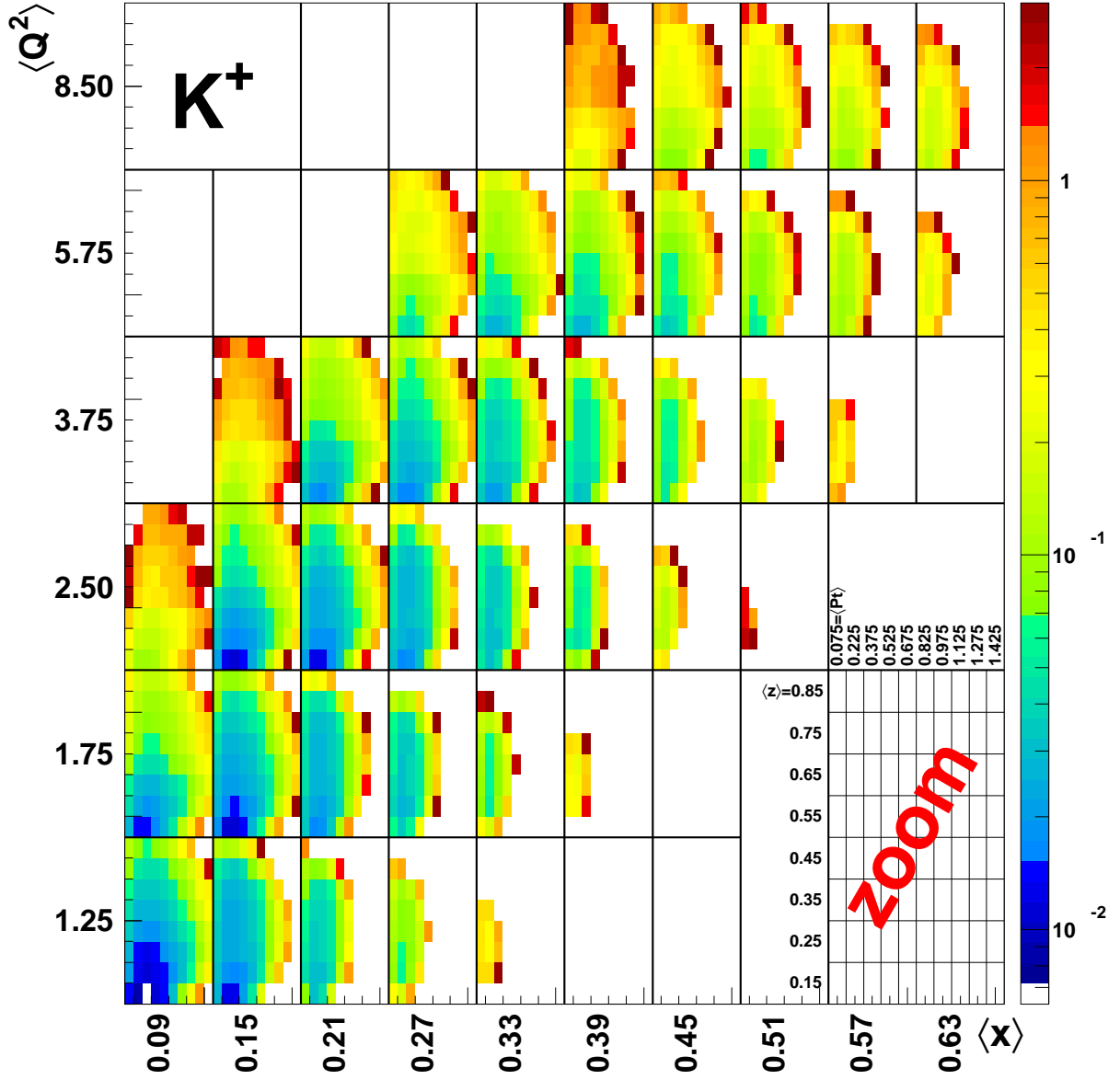


Figure 37: Expected statistical error in a 4-dimensional analysis of  $A_{UT}$  TTSA for  $K^+$ . Each  $x$ - $Q^2$  bin is subdivided in a matrix of  $z - P_T$  bins, as depicted in bottom-right corner. For each bin the average kinematical values are reported. The colors correspond to the statistical errors that can be achieved in 100 days of data-taking. Note a precision of few percents can be obtained in a large portion of the phase space.

Figs. 36-37. In the proposed data-taking time, a precise mapping of a large portion of the phase-space is achievable for pions, extending into the high- $Q^2$  high- $P_{h\perp}$  region of interest. In particular a precision of few percents can be obtained at large  $Q^2$  for values of  $P_{h\perp}$  up to 1 GeV/c. The  $x$  and  $Q^2$  variables are typically correlated by the detector acceptance. Noteworthy the statistics of the proposed experiment allows to subdivide each  $x$ -bin in several  $Q^2$ -bins thus disentangling the two kinematic dependences. An extended mapping is possible also in the kaon sector, although with a precision limited by the smaller yields.

The projected  $Q^2$ -dependence from CLAS12 data is shown in Fig. 38. Studies of the  $Q^2$  dependence will be required also to constrain the higher-twist contributions.

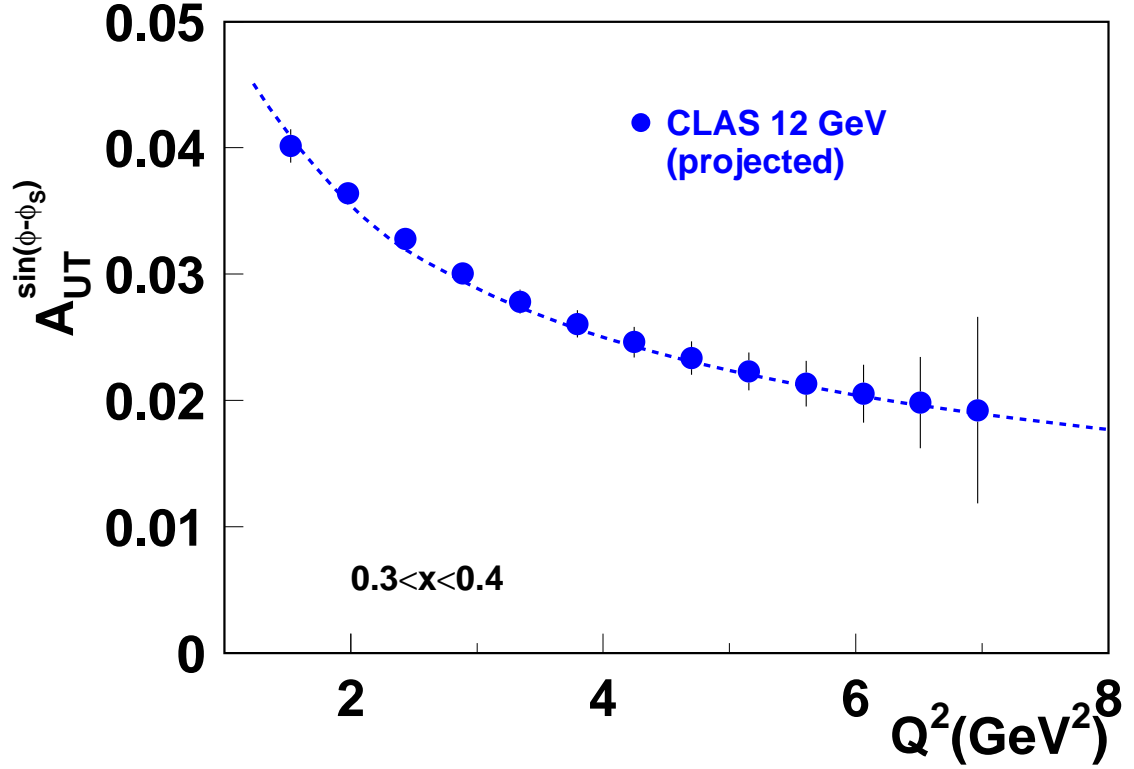


Figure 38: Projected  $Q^2$ -dependence of the Siverson asymmetry for a given bin in  $x$ . The curve corresponds to predictions based on evolution of the Siverson function [?].

## 4.4 Fourier Transformed Cross Sections

TMDs and transverse momentum-dependent fragmentation functions enter the SIDIS cross section in a convolution with respect to transverse momentum. In order to extract TMDs, it is therefore advantageous to project the differential cross section onto Fourier modes [120]. The result is a product of TMDs and fragmentation functions in Fourier space. The Fourier transform of a generic TMD  $f$  and a generic fragmentation function  $D$  is defined as

$$\tilde{f}(x, \mathbf{b}_T^2) \equiv \int d^2 \mathbf{k}_T e^{i \mathbf{b}_T \cdot \mathbf{k}_T} f(x, \mathbf{k}_T^2) = 2\pi \int d|\mathbf{k}_T| |\mathbf{k}_T| J_0(|\mathbf{b}_T| |\mathbf{k}_T|) f^a(x, \mathbf{k}_T^2), \quad (13)$$

$$\tilde{D}(z, \mathbf{b}_T^2) \equiv \int d^2 \mathbf{p}_T e^{i \mathbf{b}_T \cdot \mathbf{p}_T} D(z, \mathbf{p}_T^2) = 2\pi \int d|\mathbf{p}_T| |\mathbf{p}_T| J_0(|\mathbf{b}_T| |\mathbf{p}_T|) D^a(z, \mathbf{p}_T^2), \quad (14)$$

where  $J_0$  is a Bessel function. We also need to introduce  $\mathbf{b}_T^2$ -derivatives of the Fourier transformed distributions:

$$\begin{aligned} \tilde{f}^{(n)}(x, \mathbf{b}_T^2) &\equiv n! \left( -\frac{2}{M^2} \partial_{\mathbf{b}_T^2} \right)^n \tilde{f} = \frac{2\pi n!}{(M^2)^n} \int d|\mathbf{k}_T| |\mathbf{k}_T| \left( \frac{|\mathbf{k}_T|}{|\mathbf{b}_T|} \right)^n J_n(|\mathbf{b}_T| |\mathbf{k}_T|) f(x, \mathbf{k}_T^2), \\ \tilde{D}^{(n)}(z, \mathbf{b}_T^2) &\equiv n! \left( -\frac{2}{z^2 M_h^2} \partial_{\mathbf{b}_T^2} \right)^n \tilde{D} = \frac{2\pi n!}{(z^2 M_h^2)^n} \int d|\mathbf{p}_T| |\mathbf{p}_T| \left( \frac{|\mathbf{p}_T|}{|\mathbf{b}_T|} \right)^n J_n(|\mathbf{b}_T| |\mathbf{p}_T|) D(z, \mathbf{p}_T^2). \end{aligned} \quad (15)$$

With these definitions, we can identify the Fourier-modes of the cross section as products of the  $\tilde{f}^{(n)}$  and  $\tilde{D}^{(n)}$ . At leading twist and tree-level, we find in the  $\phi_h$ -independent channel

$$\begin{aligned} &\int_0^{2\pi} \frac{d\phi_S}{2\pi} \int_0^{2\pi} d\phi_h \int_0^\infty d|\mathbf{P}_{h\perp}| |\mathbf{P}_{h\perp}| J_0(|\mathbf{P}_{h\perp}| |\mathbf{b}_T|) \left[ \frac{d\sigma}{dx dy d\phi_S dz_h d\phi_h |\mathbf{P}_{h\perp}| d|\mathbf{P}_{h\perp}|} \right] \\ &= \frac{\alpha^2}{y Q^2} \frac{y^2}{(1-\varepsilon)} \left( 1 + \frac{\gamma^2}{2x} \right) \sum_a e_a^2 \left\{ \tilde{f}_1^{a(0)}(x, z^2 \mathbf{b}_T^2) + S_{\parallel} \lambda_e \sqrt{1-\varepsilon^2} \tilde{g}_1^{(0)a}(x, z^2 \mathbf{b}_T^2) \right\} \tilde{D}_1^{(0)a}(z, \mathbf{b}_T^2), \end{aligned}$$

where  $e_a$  is the electric charge of a quark of flavor  $a$ . The unpolarized contribution from  $f_1$  can be isolated from that of  $g_1$  by averaging over the helicity of the electron  $\lambda_e$ . The above transformation depends on the external parameter  $\mathcal{B}_T \equiv |\mathbf{b}_T|$ . Choosing different values of this parameter allows us to scan the transverse momentum dependence of the distributions in Fourier space.

A similar integration allows us to project out information on the transversity function  $h_1$ :

$$\begin{aligned} &\int_0^{2\pi} \frac{d\phi_S}{2\pi} \int_0^{2\pi} d\phi_h \sin(\phi_h + \phi_S) \int_0^\infty d|\mathbf{P}_{h\perp}| |\mathbf{P}_{h\perp}| \frac{2J_1(|\mathbf{P}_{h\perp}| |\mathbf{b}_T|)}{z M_h |\mathbf{b}_T|} \left[ \frac{d\sigma}{dx dy d\phi_S dz_h d\phi_h |\mathbf{P}_{h\perp}| d|\mathbf{P}_{h\perp}|} \right] \\ &= \frac{\alpha^2}{y Q^2} \frac{y^2}{(1-\varepsilon)} \left( 1 + \frac{\gamma^2}{2x} \right) |\mathcal{S}_\perp| \varepsilon \sum_a e_a^2 \tilde{h}_1^{(1)a}(x, z^2 \mathbf{b}_T^2) \tilde{H}_1^{\perp(1)a}(z, \mathbf{b}_T^2). \end{aligned} \quad (16)$$

A similar integration allows us to project out information on the Siverts function  $f_{1T}^\perp$ :

$$\begin{aligned} & \int_0^{2\pi} \frac{d\phi_S}{2\pi} \int_0^{2\pi} d\phi_h \sin(\phi_h - \phi_S) \int_0^\infty d|\mathbf{P}_{h\perp}| |\mathbf{P}_{h\perp}| \frac{-2J_1(|\mathbf{P}_{h\perp}||\mathbf{b}_T|)}{zM|\mathbf{b}_T|} \left[ \frac{d\sigma}{dx dy d\phi_S dz_h d\phi_h |\mathbf{P}_{h\perp}| d|\mathbf{P}_{h\perp}|} \right] \\ &= \frac{\alpha^2}{yQ^2} \frac{y^2}{(1-\varepsilon)} \left( 1 + \frac{\gamma^2}{2x} \right) |\mathbf{S}_\perp| \sum_a e_a^2 \tilde{f}_{1T}^{\perp(1)a}(x, z^2 \mathbf{b}_T^2) \tilde{D}_1^{(0)a}(z, \mathbf{b}_T^2) . \quad (17) \end{aligned}$$

A similar integration allows us to project out information on the worm gear function  $g_{1T}^\perp$ :

$$\begin{aligned} & \int_0^{2\pi} \frac{d\phi_S}{2\pi} \int_0^{2\pi} d\phi_h \cos(\phi_h - \phi_S) \int_0^\infty d|\mathbf{P}_{h\perp}| |\mathbf{P}_{h\perp}| \frac{2J_1(|\mathbf{P}_{h\perp}||\mathbf{b}_T|)}{zM|\mathbf{b}_T|} \left[ \frac{d\sigma}{dx dy d\phi_S dz_h d\phi_h |\mathbf{P}_{h\perp}| d|\mathbf{P}_{h\perp}|} \right] \\ &= \frac{\alpha^2}{yQ^2} \frac{y^2}{(1-\varepsilon)} \left( 1 + \frac{\gamma^2}{2x} \right) |\mathbf{S}_\perp| \lambda_e \sqrt{1-\varepsilon^2} \sum_a e_a^2 \tilde{g}_{1T}^{(1)a}(x, z^2 \mathbf{b}_T^2) \tilde{D}_1^{(0)a}(z, \mathbf{b}_T^2) . \quad (18) \end{aligned}$$

A similar integration allows us to project out information on the Pretzelosity function  $h_{1T}^\perp$ :

$$\begin{aligned} & \int_0^{2\pi} \frac{d\phi_S}{2\pi} \int_0^{2\pi} d\phi_h \sin(3\phi_h - \phi_S) \int_0^\infty d|\mathbf{P}_{h\perp}| |\mathbf{P}_{h\perp}| \frac{8J_3(|\mathbf{P}_{h\perp}||\mathbf{b}_T|)}{z^3 M^2 M_h |\mathbf{b}_T|^3} \left[ \frac{d\sigma}{dx dy d\phi_S dz_h d\phi_h |\mathbf{P}_{h\perp}| d|\mathbf{P}_{h\perp}|} \right] \\ &= \frac{\alpha^2}{yQ^2} \frac{y^2}{(1-\varepsilon)} \left( 1 + \frac{\gamma^2}{2x} \right) |\mathbf{S}_\perp| \varepsilon \sum_a e_a^2 \tilde{h}_{1T}^{\perp(2)a}(x, z^2 \mathbf{b}_T^2) \tilde{H}_1^{\perp(1)a}(z, \mathbf{b}_T^2) . \quad (19) \end{aligned}$$

The formalism in  $\mathbf{b}_T$ -space avoids convolutions, making it easier to perform a model independent analysis. The fundamental objects in this formalism are the (derivatives of) Fourier transformed TMDs  $\tilde{f}_1^{(0)}, \tilde{g}_1^{(0)}, \tilde{h}_1^{(0)}, \tilde{f}_{1T}^{\perp(1)}, \tilde{g}_{1T}^{(1)}, \tilde{h}_1^{\perp(1)}, \tilde{h}_{1L}^{\perp(1)}, \tilde{h}_{1T}^{\perp(2)}$  and fragmentation functions  $\tilde{D}_1^{(0)}, \tilde{H}_1^{\perp(1)}$ . Theoretically, these  $|\mathbf{b}_T|$ -dependent distributions contain the same information as their conventional, momentum-dependent counterparts. In practice, however, only a limited range in  $|\mathbf{b}_T|$  is accessible with sufficient accuracy from experiments. Thus, to carry out the Fourier transformation back to conventional TMDs, model assumptions must be made in order to supplement information over the whole range of  $|\mathbf{b}_T|$ .

The  $|\mathbf{b}_T|$ -dependent distributions are also the objects that appear in the evolution equations that describe the scale dependence beyond tree level, see, e.g., Ref. [121]. Lattice calculations of TMDs are performed in  $b$ -space rather than momentum space as well [57, 58]. This suggests that it is the  $|\mathbf{b}_T|$ -dependent quantities that are most suitable for a model independent analysis and comparison with lattice data.

The main questions to address when applying this procedure to CLAS12 data are the limited range in hadron transverse momenta and the low  $Q^2$ , as Fourier-transformed quantities receive (through the Fourier integral) contributions from the entire range of  $P_{h\perp}$ , while the whole factorization formalism requires  $P_{h\perp} \ll Q$ . The effect of the cut on the maximum value of  $P_{h\perp}$  is shown in Fig. 39. Due to

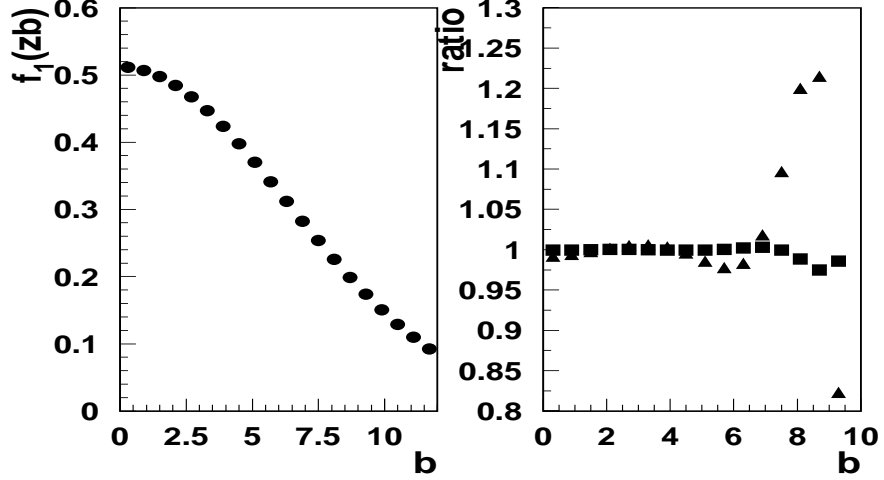


Figure 39: Extracted Fourier transformed  $f_1$  from unpolarized MC with Gaussian widths for  $f_1$  and  $D_1$  assumed as  $0.2 \text{ GeV}^2$  and  $0.25 \text{ GeV}^2$ , respectively, and average  $x$  and  $z$  at 0.2 and 0.5, respectively. The ratio is defined as the ratio of Fourier transformed  $b$ -dependences for integrals over  $k_T$  for  $P_{h\perp} < P_{T_{max}}$  and the full  $P_{h\perp}$ -integration. Squares and triangles correspond to  $P_{T_{max}} = 1.5$  and  $1.2 \text{ GeV}$ , respectively.

contributions to the cross section at high  $|\mathbf{P}_{h\perp}|$  that are not accounted for in the TMD factorized framework, further studies are needed as to whether and in what range of  $\mathbf{b}_T$  we can extract TMDs in Fourier space at JLab kinematics with moderate theoretical uncertainties. Most likely, precision measurements at large  $\mathbf{b}_T$  will require precision measurements at  $P_{h\perp}$  in the range of 1.2-1.5 GeV, limiting the minimum  $Q^2$  to at least  $2 \text{ GeV}^2$ .

## 5 Summary and Beam Time Request

In this experiment we propose a study of the Transverse Momentum-Dependent (TMD) parton distributions via measurements of pion and kaon electro-production in SIDIS in the hard scattering regime ( $Q^2 > 1 \text{ GeV}^2$ ,  $W^2 > 4 \text{ GeV}^2$ ), using an 11 GeV electron beam from the upgraded CEBAF facility and the CLAS12 detector.

For this proposal, we request 110 days of beam time with high polarization of electrons at 11 GeV and a transversely polarized hydrogen target (100 days of data-taking plus 10 days for calibration, empty target runs and supportive tests). We expect to improve substantially the statistical precision of the HERMES measurements on the hydrogen target and the COMPASS measurements on the deuterium and proton targets, especially in the intermediate-to-large  $x$  region ( $x > 0.2$ ). The precise mapping of the valence region is important to extract fundamental quantities like the tensor charge [87, 122], which can be compared to Lattice QCD calculations [123].

The large acceptance of the CLAS12 detector permits a simultaneous scan of various variables ( $x$ ,  $z$ ,  $P_T$  and  $Q^2$ ). The most important advantage of the HD-Ice target compared to nuclear targets ( $\text{NH}_3$ ,  $\text{ND}_3$ ) is its superior dilution factor, crucial for studies of transverse momentum dependence of TMDs, which is one of the main goals of our proposal. Wide acceptance of the HD-Ice also increases the kinematical coverage of measurements, in particular at large  $Q^2$ , providing a wider range in  $Q^2$  to study evolution effects and control possible higher twist contributions in the measurements of TMD observables in general, and of the Sivers asymmetry in particular.

Analysis of already existing electroproduction data from CLAS with unpolarized and longitudinally polarized targets has shown that the proposed measurements are feasible. Combined analysis of all three data sets will constrain different TMDs and relations between them, providing important input to global analysis of PDFs and will provide a substantial contribution to *nucleon tomography*.

### Beam Request

**We ask the PAC to award 110 days of beam time for a dedicated high statistics SIDIS experiment with the transversely polarized target.**

The measurement will produce precise data on the underlying quark transverse momentum distributions, providing important information on spin-orbit correlations.

## References

- [1] J.P. Ralston and D.E. Soper, Nucl. Phys. B152 (1979) 109.
- [2] D.W. Sivers, Phys. Rev. D41 (1990) 83.
- [3] A. Kotzinian, Nucl. Phys. B441 (1995) 234, hep-ph/9412283.
- [4] P.J. Mulders and R.D. Tangerman, Nucl. Phys. B461 (1996) 197, hep-ph/9510301.
- [5] D. Boer and P.J. Mulders, Phys. Rev. D57 (1998) 5780, hep-ph/9711485.
- [6] P.J. Mulders and J. Rodrigues, Phys. Rev. D63 (2001) 094021, hep-ph/0009343.
- [7] A.V. Belitsky, X.d. Ji and F. Yuan, Phys. Rev. D69 (2004) 074014, hep-ph/0307383.
- [8] A. Bacchetta et al., JHEP 02 (2007) 093, hep-ph/0611265.
- [9] M. Burkardt, Phys. Rev. D62 (2000) 071503, hep-ph/0005108.
- [10] K. Goeke, M.V. Polyakov and M. Vanderhaeghen, Prog. Part. Nucl. Phys. 47 (2001) 401, hep-ph/0106012.
- [11] M. Burkardt, Int. J. Mod. Phys. A18 (2003) 173, hep-ph/0207047.
- [12] M. Diehl, Phys. Rept. 388 (2003) 41, hep-ph/0307382.
- [13] X. Ji, Ann. Rev. Nucl. Part. Sci. 54 (2004) 413.
- [14] A.V. Belitsky and A.V. Radyushkin, Phys. Rept. 418 (2005) 1, hep-ph/0504030.
- [15] S. Boffi and B. Pasquini, Riv. Nuovo Cim. 30 (2007) 387, 0711.2625.
- [16] X.d. Ji, Phys. Rev. Lett. 91 (2003) 062001, hep-ph/0304037.
- [17] S.J. Brodsky, D.S. Hwang and I. Schmidt, Phys. Lett. B530 (2002) 99, hep-ph/0201296.
- [18] J.C. Collins, Phys. Lett. B536 (2002) 43, hep-ph/0204004.
- [19] X. Ji and F. Yuan, Phys. Lett. B543 (2002) 66, hep-ph/0206057.
- [20] A.V. Belitsky, X. Ji and F. Yuan, Nucl. Phys. B656 (2003) 165, hep-ph/0208038.
- [21] D. Boer, S.J. Brodsky and D.S. Hwang, Phys. Rev. D67 (2003) 054003, hep-ph/0211110.

- [22] D. Boer, P.J. Mulders and F. Pijlman, Nucl. Phys. B667 (2003) 201, hep-ph/0303034.
- [23] X. Ji, J. Ma and F. Yuan, Phys. Rev. D71 (2005) 034005, hep-ph/0404183.
- [24] J.C. Collins and A. Metz, Phys. Rev. Lett. 93 (2004) 252001, hep-ph/0408249.
- [25] K. Goeke, A. Metz and M. Schlegel, Phys. Lett. B618 (2005) 90, hep-ph/0504130.
- [26] S. Meissner, A. Metz and K. Goeke, Phys. Rev. D76 (2007) 034002, hep-ph/0703176.
- [27] C. Lorce and B. Pasquini, (2011), 1104.5651.
- [28] J.C. Collins, Nucl. Phys. B396 (1993) 161, hep-ph/9208213.
- [29] S.J. Brodsky, D.S. Hwang and I. Schmidt, Nucl. Phys. B642 (2002) 344, hep-ph/0206259.
- [30] Z.B. Kang and J.W. Qiu, Phys. Rev. Lett. 103 (2009) 172001, 0903.3629.
- [31] H. Avakian et al., JLab Experiment E12-06-112 (2006).
- [32] H. Avakian et al., JLab Experiment E12-09-008 (2009).
- [33] H. Avakian et al., JLab Experiment E12-07-107 (2007).
- [34] H. Avakian et al., JLab Experiment E12-09-009 (2009).
- [35] COMPASS, A. Kotzinian, (2007), arXiv:0705.2402 [hep-ex].
- [36] COMPASS, P. Abbon et al., Nucl. Instrum. Meth. A577 (2007) 455, hep-ex/0703049.
- [37] R.L. Jaffe and X.D. Ji, Nucl. Phys. B375 (1992) 527.
- [38] E. Leader, A.V. Sidorov and D.B. Stamenov, Phys. Lett. B462 (1999) 189, hep-ph/9905512.
- [39] H.C. Kim, M.V. Polyakov and K. Goeke, Phys. Lett. B387 (1996) 577, hep-ph/9604442.
- [40] M. Anselmino et al., Phys. Rev. D71 (2005) 074006, hep-ph/0501196.
- [41] J.C. Collins et al., Phys. Rev. D73 (2006) 094023, hep-ph/0511272.
- [42] W. Vogelsang and F. Yuan, Phys. Rev. D72 (2005) 054028, hep-ph/0507266.

- [43] M. Anselmino et al., hep-ph/0805.2677 (2008), hep-ph/0805.2677.
- [44] I.O. Cherednikov and N.G. Stefanis, Phys. Rev. D77 (2008) 094001, 0710.1955.
- [45] I.O. Cherednikov and N.G. Stefanis, Nucl. Phys. B802 (2008) 146, 0802.2821.
- [46] I.O. Cherednikov and N.G. Stefanis, Phys. Rev. D80 (2009) 054008, 0904.2727.
- [47] Fermilab E906/SeaQuest, P. Reimer et al., (2001), Fermilab Proposal 906, Unpublished, <http://projects-docdb.fnal.gov/cgi-bin/RetrieveFile?docid=402>.
- [48] E906/SeaQuest, P. Reimer et al., (2006), Experiment update to Fermilab PAC <http://projects-docdb.fnal.gov/cgi-bin/ShowDocument?docid=395>.
- [49] L. et al., (2011), [http://www.bnl.gov/npp/docs/pac0611/DY\\_pro\\_110516\\_final.2.pdf](http://www.bnl.gov/npp/docs/pac0611/DY_pro_110516_final.2.pdf).
- [50] D. Boer, (2011), 1105.2543.
- [51] H. Mkrtchyan et al., Phys. Lett. B665 (2008) 20, hep-ph/0709.3020.
- [52] The CLAS, H. Avakian et al., Phys. Rev. Lett. 105 (2010) 262002, hep-ex/1003.4549.
- [53] Z. Lu and B.Q. Ma, Nucl. Phys. A741 (2004) 200, hep-ph/0406171.
- [54] M. Anselmino et al., Phys. Rev. D74 (2006) 074015, hep-ph/0608048.
- [55] B. Pasquini, S. Cazzaniga and S. Boffi, Phys. Rev. D78 (2008) 034025, hep-ph/0806.2298.
- [56] C. Bourrely, F. Buccella and J. Soffer, (2010), 1008.5322.
- [57] P. Hagler et al., Europhys. Lett. 88 (2009) 61001, hep-lat/0908.1283.
- [58] B.U. Musch et al., (2010), 1011.1213.
- [59] Z.B. Kang et al., Phys. Rev. D83 (2011) 094001, 1103.1591.
- [60] G.A. Miller, Phys. Rev. C76 (2007) 065209, nucl-th/0708.2297.
- [61] M. Burkardt, hep-ph 0709.2966 (2007), hep-ph/0709.2966.
- [62] J. She, J. Zhu and B.Q. Ma, Phys. Rev. D79 (2009) 054008, 0902.3718.
- [63] H. Avakian et al., (2008), hep-ph/0805.3355.
- [64] H. Avakian et al., Phys. Rev. D81 (2010) 074035, hep-ph/1001.5467.
- [65] H. Avakian et al., Mod. Phys. Lett. A24 (2009) 2995, 0910.3181.

- [66] M. Burkardt and H. BC, Phys. Rev. D79 (2009) 071501, 0812.1605.
- [67] X.D. Ji, Phys. Rev. Lett. 78 (1997) 610, hep-ph/9603249.
- [68] P. Schweitzer, T. Teckentrup and A. Metz, Phys. Rev. D81 (2010) 094019, 1003.2190.
- [69] S. Boffi et al., Phys. Rev. D79 (2009) 094012, hep-ph/0903.1271.
- [70] B. Pasquini and F. Yuan, Phys. Rev. D81 (2010) 114013, 1001.5398.
- [71] B.U. Musch, (2009), 0907.2381.
- [72] H. Avakian et al., JLab Experiment E12-09-007 (2009).
- [73] X.d. Ji, J.P. Ma and F. Yuan, Phys. Lett. B597 (2004) 299, hep-ph/0405085.
- [74] X. Ji et al., Phys. Rev. D73 (2006) 094017, hep-ph/0604023.
- [75] J.w. Qiu and G.F. Sterman, Phys. Rev. Lett. 67 (1991) 2264.
- [76] E581, D.L. Adams et al., Z. Phys. C56 (1992) 181.
- [77] STAR, J. Adams et al., Phys. Rev. Lett. 92 (2004) 171801, hep-ex/0310058.
- [78] A.M. Kotzinian and P.J. Mulders, Phys. Rev. D54 (1996) 1229, hep-ph/9511420.
- [79] A. Bacchetta et al., JHEP 08 (2008) 023, hep-ph/0803.0227.
- [80] HERMES, A. Airapetian et al., Phys. Rev. Lett. 94 (2005) 012002, hep-ex/0408013.
- [81] COMPASS, V.Y. Alexakhin et al., Phys. Rev. Lett. 94 (2005) 202002, hep-ex/0503002.
- [82] COMPASS, E.S. Ageev et al., Nucl. Phys. B765 (2007) 31, hep-ex/0610068.
- [83] HERMES, A. Airapetian et al., Phys. Lett. B693 (2010) 11, 1006.4221.
- [84] The COMPASS, M.G. Alekseev et al., Phys. Lett. B692 (2010) 240, 1005.5609.
- [85] M.G. Alekseev et al., Eur. Phys. J. C70 (2010) 39, 1007.1562.
- [86] C.f.C. Schill, (2011), DIS 2011 Conference.
- [87] M. Anselmino et al., Nucl. Phys. Proc. Suppl. 191 (2009) 98, 0812.4366.
- [88] HERMES, A. Airapetian et al., Phys. Rev. Lett. 103 (2009) 152002, 0906.3918.

- [89] Belle, K. Abe et al., Phys. Rev. Lett. 96 (2006) 232002, hep-ex/0507063.
- [90] Belle, A. Ogawa et al., AIP Conf. Proc. 915 (2007) 575.
- [91] Belle, R. Seidl et al., Phys. Rev. D78 (2008) 032011, 0805.2975.
- [92] A. Bacchetta et al., Phys. Rev. D65 (2002) 094021, hep-ph/0201091.
- [93] A.V. Efremov, K. Goeke and P. Schweitzer, Phys. Rev. D67 (2003) 114014, hep-ph/0208124.
- [94] A.M. Kotzinian et al., (1999), hep-ph/9908466.
- [95] M. Anselmino et al., (2007), hep-ph/0701006.
- [96] COMPASS, B. Parsamyan, Eur. Phys. J. ST 162 (2008) 89, 0709.3440.
- [97] H. Avakian et al., Phys. Rev. Lett. 99 (2007) 082001, hep-ph/0705.1553.
- [98] HERMES, A. Airapetian et al., Phys. Lett. B562 (2003) 182, hep-ex/0212039.
- [99] J.C. Collins et al., Phys. Rev. D73 (2006) 014021, hep-ph/0509076.
- [100] European Muon, M. Arneodo et al., Z. Phys. C34 (1987) 277.
- [101] BELLE Collaboration, R. Seidl et al., Phys.Rev. D78 (2008) 032011.
- [102] I. Garzia et al., Nuovo Cimento 33C (2010) 269.
- [103] R.L. Jaffe, Int. J. Mod. Phys. A18 (2003) 1141, hep-ph/0201068.
- [104] D.W. Sivers, Phys. Rev. D43 (1991) 261.
- [105] J. Zhu and B.Q. Ma, (2011), 1104.5545.
- [106] Hall-A, . X.Jiang et al., Hall-A proposal E06-010 (2006).
- [107] H. Avakian et al., JLab Experiment E12-07-015 (2008).
- [108] H. Avakian et al., JLab Experiment E12-06-015 (2008).
- [109] G. Cates et al., JLab Experiment E12-11-007 (2008).
- [110] H. Hao, Q. X. and P. J.-C., JLab Experiment E12-11-007 (2008).
- [111] H. Gao et al., Eur. Phys. J. Plus 126 (2011) 2, 1009.3803.
- [112] H. Gao et al., PAC38 Hall-A proposal: Target SSA in SIDIS with transversely polarized  $\text{NH}_3$  (2011).

- [113] W.K. Brooks and H. Hakobyan, Nucl. Phys. A830 (2009) 361c, 0907.4606.
- [114] CLAS, . A.Sandorfi et al., CLAS proposal E06-101 (2006).
- [115] A. Caracappa and C. Thorn, AIP Conf. Proc. 675 (2003) 867.
- [116] C. Thorn and . Caracappa, AIP Conf. Proc. (2007) (in press).
- [117] Jefferson Lab Hall A, M.K. Jones et al., Phys. Rev. Lett. 84 (2000) 1398, nucl-ex/9910005.
- [118] A. Efremov et al., AIP Conf.Proc. 1149 (2009) 547, 0812.3246.
- [119] A. Kotzinian, B. Parsamyan and A. Prokudin, Phys. Rev. D73 (2006) 114017, hep-ph/0603194.
- [120] D. Boer et al., (2011), in preparation.
- [121] A. Idilbi et al., Phys. Rev. D70 (2004) 074021, hep-ph/0406302.
- [122] M. Wakamatsu, Phys. Rev. D79 (2009) 0140338, 0811.4196.
- [123] M. Goeckeler et al., Phys. Lett. B627 (2005) 113, 0507001.